Optimal continuation power flow

by

Ping Lin Ronnie Lau

A Thesis Submitted to the

Graduate Faculty in Partial Fulfillment of the

Requirements for the Degree of

MASTER OF SCIENCE

Department : Electrical Engineering and Computer Engineering
Major: Electrical Engineering

Iowa State University
Ames, Iowa
1991

TABLE OF CONTENTS

LIST OF TABLES

LIST OF FIGURES

1 INTRODUCTION

1.1 The Phenomena of Voltage Collapse

Two decades ago, the problem related to the presence of reactive power in power system was not a major concern. Mainly, the control of voltage could easily be achieved in an almost entirely decentralized manner. By using local reactive resources such as generators, synchronous condensers and various tap changers, the voltage levels at certain buses could be regulated through preassigned setpoints. To follow the daily load variation, it was sufficient to change the voltage setpoints several times a day or to switch some of the capacitors and reactors in and out at certain times during the day. As a result, the relationship between reactive power and voltage was not studied in detail and fully understood.

Meanwhile, the flow of power because of various economic reasons and related issues started to increase dramatically causing the transmission and distribution networks to reach their maximum capacity limits at a rapid rate. The problem of voltage or reactive instability became more visible and imminent. For example, the 1978 French blackout and the Tokyo blackout in 1987 that lasted for some 20 minutes were related to the problem of insufficient reactive support. The term "voltage collapse" was then commonly adopted to describe the

process by which voltage instability leads to loss of voltage in a significant part of a system.

Almost twenty years have already gone by, extensive research are still undertaking to understand and analyze the nature of these phenomena. The need to develop operating and control practices to assure security, viability and stability from the aspect of voltage-reactive power in the power systems has become greater and more urgent.

To prevent voltage collapse from occurring, power system operators are looking for tools that can enhance their understanding of where the system is actually operating with respect to point of voltage collapse. In the literature, this point is generally referred to as the critical point. See Figure 1.1.

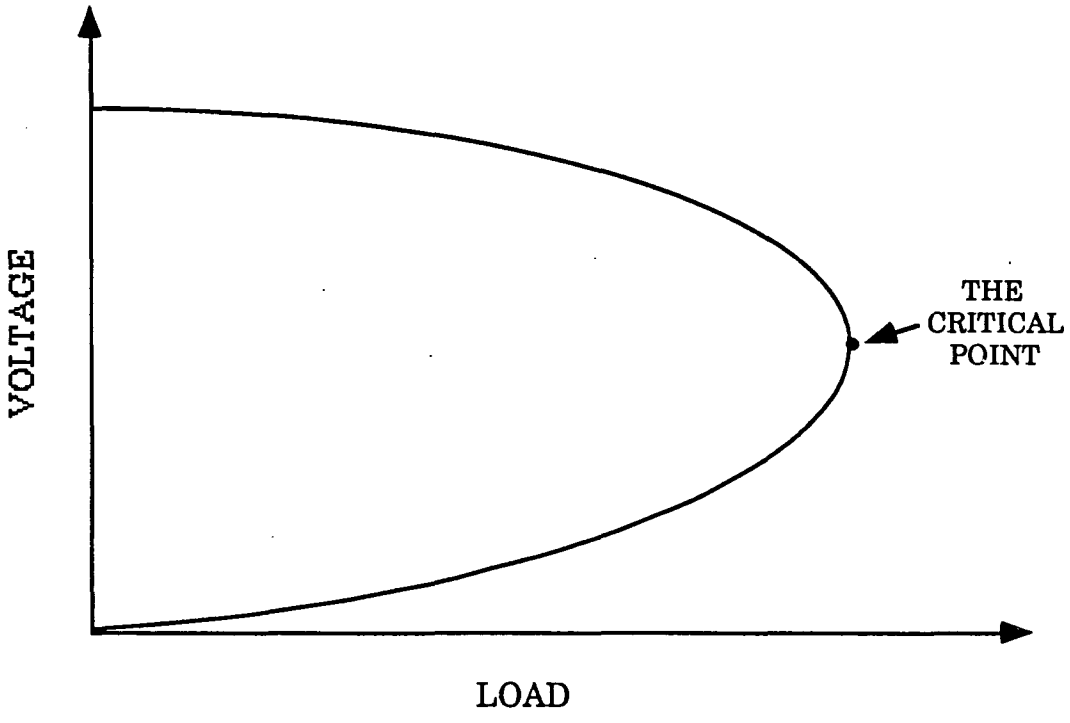

Figure 1.1: Illustration of the critical point on a P-V curve

The critical point is best illustrated by plotting the relationship between real power and voltage at a load bus of a 2-bus system. The result is a P-V curve (nose curve) with the critical point located at the tip of the curve.

In this research, the problem of voltage instability, which causes the phenomenon of voltage collapse, is examined from the steady-state perspective.

1.2 Causes of Voltage Collapse

When transmission systems are highly interconnected and heavily loaded, power systems become more stressed and vulnerable. A close look at the problem reveals that the causes of today's stressed power systems are many and often involve complex issues. For examples, the high cost of upgrading existing transmission lines to meet increasing energy consumption; the difficulty of acquiring right-of-way from landowners; the delay of obtaining license to build new transmission lines; the increasing concern of the electromagnetic field (EMF) to human health; the shift of generation pattern because of environmental constraints; the bulk power transfer from remote generation sites to load centers over long distances.

With the advent of full utilization of transmission for economic transfer, many electric utilities are being driven to operate their systems close to either the thermal limit or the steady-state voltage stability limit. The tasks of maintaining adequate control and stable voltage within permissible operating limits have become increasingly difficult.

In general, maintaining voltage in power system requires reactive power support. However, reactive power cannot be transported over long distance. This leads to the necessity of supplying reactive power at points of system remote from generation and usually close to or within major load centers.

Voltage collapse is a local phenomenon; but if proper actions are not taken in time, it can spread over a wide area and create cascaded outages. Characterized by a progressive decline in voltage magnitudes, voltage collapse is commonly associated with the lack of or the loss of reactive power supply for voltages at certain buses in a stressed power system. This phenomenon is often triggered by some form of disturbance or contingency causing changes in reactive power requirements at certain locations within the system. The sudden loss of a major transmission line because of automatic tripping is a good example. Figure 1.2 depicts a possible scenario with a sequence of events that may lead to voltage collapse.

1.3 Incidents and Current Preventive Measures

This voltage collapse phenomenon, which contributed to blackouts and brownouts of various degrees, has been reported in many countries with losses in the millions of dollars. Table 1.1 shows some of the past incidents related to voltage collapse [1].

As a consequence, it has become one of the major concerns among the electric utilities. Unfortunately, many electric utilities are still relying on

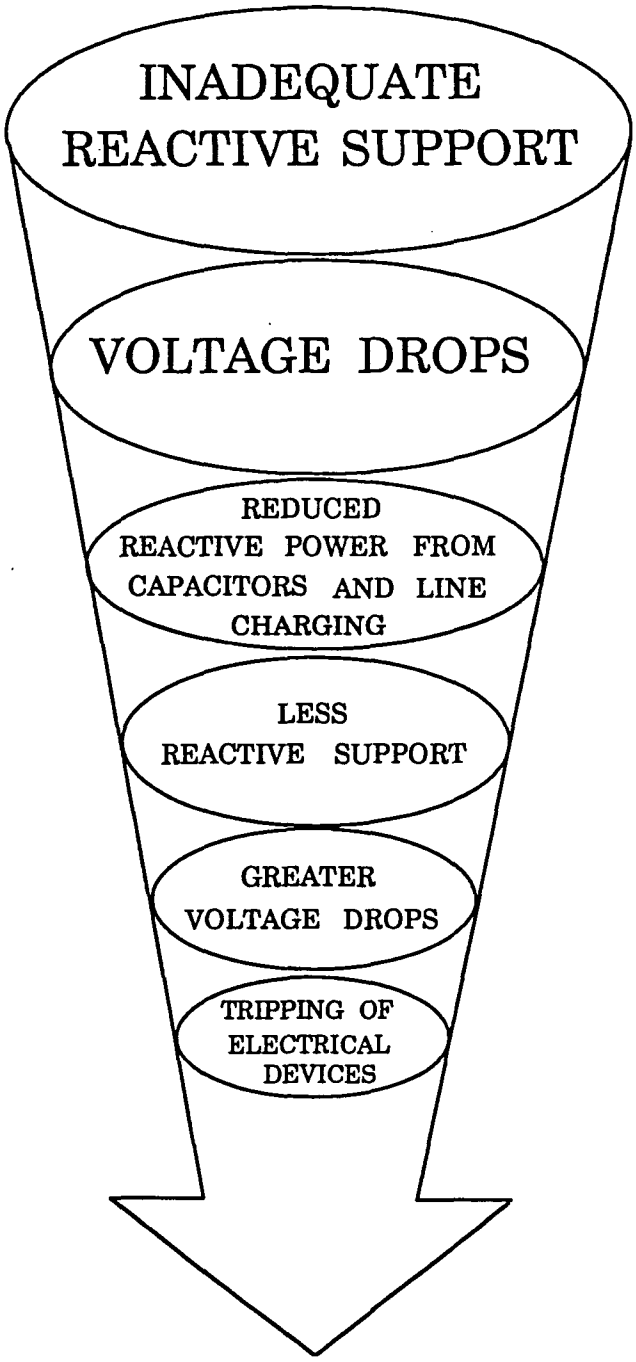

Figure 1.2: The voltage collapse phenomenon

Table 1.1: Incidents of voltage collapse [1]

Date	Location	Time Frame
11/30/86	SE Brazil, Paraguay	2 seconds
5/17/85	South Florida	4 seconds
8/22/87	Memphis, Tennessee	10 seconds
12/27/83	Sweden	50 seconds
7/79	British Col. north coast	1 minute
9/2/82	Florida	1-3 minutes
11/26/82	Florida	1-3 minutes
12/28/82	Florida	1-3 minutes
12/30/82	Florida	2 minutes
9/22/77	Jacksonville, Florida	few minutes
8/4/82	Belgium	4.5 minutes
12/9/65	Brittany, France	?
11/10/76	Brittany, France	?
7/23/87	Tokyo	20 minutes
12/19/78	France	26 minutes
8/22/70	Japan	30 minutes

the results obtained from the multiple runs of power flow and stability programs to analyze potential voltage collapse situations.

As a preventive measure, engineers may have to simulate numerous anticipated load growth scenarios. Using proper load modelling along with reactive power compensation at selected locations, engineers may then be able to establish a list of guidelines or perhaps some form of margins for the operators to follow. However, this requires good engineering judgement and knowledge of the system characteristics in order to deal effectively with voltage instability. Furthermore, this approach provides neither sensitivity information nor insights into the degree of stability or instability.

Meanwhile, system operators have to ensure bus voltages below critical values and constantly monitor remaining reactive reserves in the system. In case

of emergency, the operator will have to activate possible reactive reserve within the nearby vicinity. If all the reactive reserve are exhausted, system operators may have to limit power flow into the troubled area or curtail load within the area.

However, the automatic control action taken by the load tap changer (LTC) can produce destabilizing effect and aggravate the collapse process. Under such conditions, the LTCs involved should be blocked and, possibly, load shedding will be required to maintain the integrity of the overall power system network.

1.4 Technical and Numerical Difficulties

In the case of a heavy loading condition and the loss of transmission lines or reactive power sources, the excessive amount of reactive power that must flow over the remaining lines will create substantial voltage drops. These voltage drops will reduce the output of the existing non-synchronous capacitive sources, which in turn will accelerate the process of voltage collapse. One method of keeping the system intact is to deploy reactive support at various strategic locations. This will increase the reliability of the system and reduce the installation costs.

Nevertheless, reactive power support itself cannot eliminate the entire problem. For instance, the detection for impending voltage collapse can easily be impaired by injecting excessive amount of reactive support. In which case,

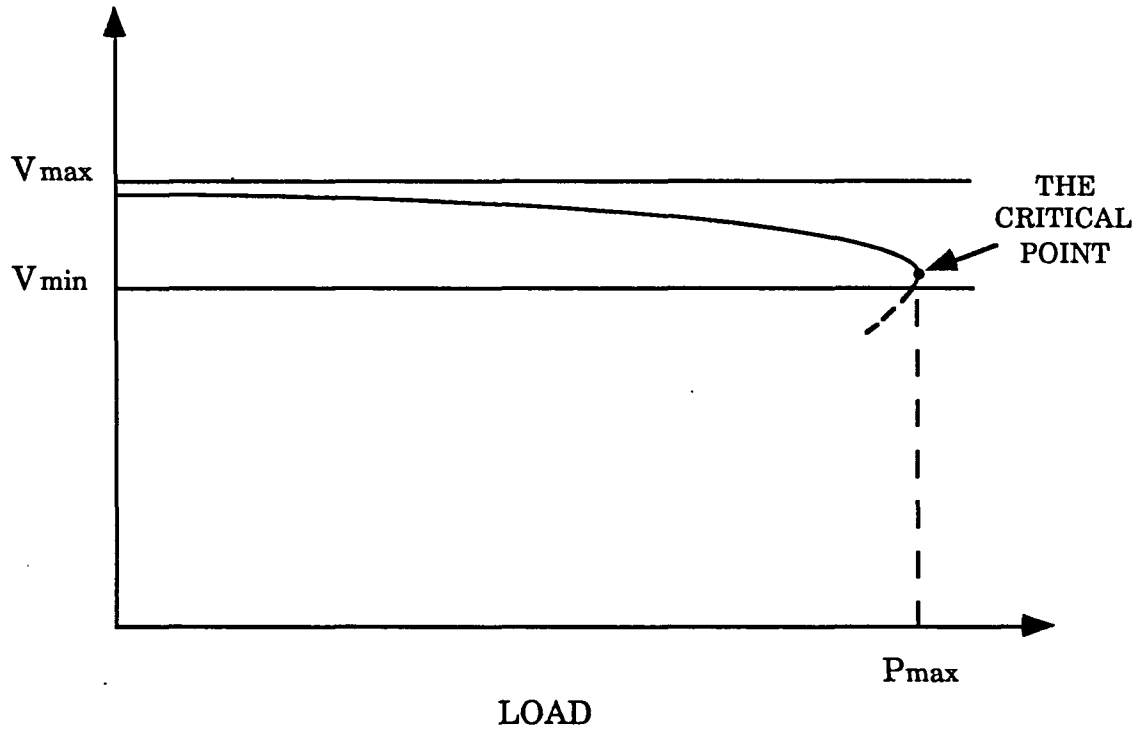

Figure 1.3: Effect of over reactive support on system voltage

voltage magnitudes may not drop below acceptable levels while the system approaches its critical state as shown in Figure 1.3. Clearly, it is possible for the critical point to lie dangerously close to the permissible voltage limits without any early warning. Therefore, using voltage magnitudes as a measure to detect voltage collapse is not sufficient or reliable.

One way to avoid voltage collapse is to locate the critical point so that a security assessment can be made. However, the search for such a critical point is not straightforward. The power flow solution diverges at the critical point as a result of singularity in the Jacobian matrix of the Newton-Raphson power flow formulation. This creates an extra barrier to the study of voltage collapse.

Another way to detect the critical point is to calculate the eigenvalues. When any one of the eigenvalues becomes zero, the critical point has been reached. However, performing eigenvalue analysis is computational expensive.

1.5 Literature Review

During the past two decades, numerous researchers had devoted their attention to the problem of voltage collapse. The following are some of the literature that are pertinent to this research.

To avoid numerical ill-conditioning associated with the singularity of the Jacobian matrix, the authors in [2] and [3] formulated the search for the critical point as an optimization problem of maximizing the system load level while taking consideration of the generators' limits. Similar to those proposed in [4,5] which try to calculate the singularity point directly, Van Custem [2] and Obadina [3] formulated a security margin following the calculation of the critical point. Based upon this result, Obadina extended his work in [6] to minimize the cost of VAr supply to reach the maximum load level for a desired security margin. Unfortunately, the author overlooked the effect of VAr once it was injected. A solution path that was different from the one generated by the process of optimization would result. This caused the critical point to move and settle at a new and greater system load level. Consequently, the maximum load level obtained would be far more conservative than it was anticipated.

Some researchers explored other possibilities to avoid the problem of singularity. For example, Semlyen in [7] chose to express the increased loading

by increasing the admittances of the loads. A formulation with $Y_{Load} = Y_{Load0} + \mu\Delta Y_{Load}$ was developed where the loading parameter μ permits continuous advancement in load level along the P-V curve regardless of the collapse point. Meanwhile, Iba in Japan [8] applied the Homotopy Continuation Method to detect the critical point. A homotopy parameter was introduced and used to trace the curve of solutions from a base load condition to a critical load condition without experiencing numerical ill-conditioning. This latter method is very similar to the continuation method developed at Iowa State University using a predictor-corrector procedure [9].

1.6 Motivation

In response to the need for an analytical tool to protect against voltage collapse, a continuation power flow program was developed at Iowa State University [9] in an attempt to offer a detailed steady-state analysis of the voltage collapse phenomena. This power flow program, which allows approximate calculation of the critical point, offers valuable sensitivity information concerning the differential change of voltage or angle in response to the differential change of system load. Through the sensitivity information, weak buses that are prone to voltage collapse can be identified easily [10].

Initially, the continuation power flow program starts at a base load with a specified load increase scenario. In one program run, the continuation power flow provides a series of power flow solutions up to and slightly past the critical

point. For each calculated power flow solution, the continuation power flow will produce

a) An index to tell the distance from the critical point

b) A list of weak buses most prone to voltage collapse

The motivation behind this research is to make use of the weak bus information in a planning environment to determine possible remedial actions and improvements on the level of the power transfer capability. Since the real power transfer capability of a system can be improved by the injection of reactive power, it is of interest to determine how much reactive power support is required and where it's location so that both a secure and economical solution can be achieved.

1.7 Scope and Objective of This Thesis

The first objective of this research is to maximize the real power transfer of a given power system with minimum amount of shunt reactive power support before voltage collapse. It is a problem that involves conflicting objectives; since maximizing the real power transfer implies maximizing the reactive power support. The second objective of this research is to preserve the validity of the voltage stability index while the first objective is being sought. In addition, this research seeks to establish a security margin against voltage collapse.

The remainder of this thesis is contained in five additional chapters. Chapter 2 introduces the relationships between the voltage and the reactive power in a power system. Then, the principles behind the continuation power

flow are carefully reviewed in Chapter 3. Since optimization and power flow techniques are required in this research, Chapter 4 is designed to give an overview of the optimal power flow. After the basic principles have been reviewed, Chapter 5 discusses the strategy undertaken in this research along with the corresponding results. Meanwhile, the idea of a security margin is incorporated and the experiences gained from the various test systems are gathered in the assessment section for further discussion. Finally, Chapter 6 summaries the approach and identifies related topics for future research.

2 VOLTAGE AND REACTIVE POWER RELATIONSHIPS

2.1 Introduction

In this chapter, a review of the tools for voltage and reactive power control is presented along with the characteristics of reactive power. The definitions and concepts of voltage instability, voltage security and voltage collapse are defined. To demonstrate some of the fundamental concepts, a 2-bus system is used. A direct method that can calculate the critical point in a exact manner is also introduced in the final section.

2.2 Controls of Voltage and Reactive Power

In a typical electric power system, there exist a wide variety of control tools for maintaining desired voltage and reactive flow levels under changing operating conditions. The following is a list of those tools and methods:

1) Synchronous generators
2) Synchronous condensers
3) Under load tap changing transformers
4) Shunt capacitor banks

5) Series capacitor banks
6) Thyristor controlled reactors and capacitors - static VAr compensator (SVC)
7) Voltage regulators
8) Phase shifting transformers
9) Fixed tap transformers
10) Line dropping
11) Load dropping
12) Voltage reduction

where the last three items are mostly for emergency control measurements.

Series capacitors, on the other hand, are mainly inserted at intervals in long transmission lines to alter the line's reactive characteristics. This has the effect of shortening the electrical distance between buses. Unlike shunt capacitors, the problem of overvoltage at low load levels is avoided since the voltage support is a function of the load current passing through the series capacitors. Although series capacitors have the advantage of simplicity, they lack the controllability of reactive compensation. In some situations, series capacitors are also responsible for the subsynchronous resonance problems.

The main advantage of using SVCs is that they offer a variety of reactive compensation capabilities through thyristor controlled reactors and capacitors. Often, SVCs are preferred for heavy and changing loads. The functions of SVC are: 1) to maintain voltage at or near a constant level; 2) to improve power system stability; 3) to improve power factor and correct phase unbalance [11].

When considering the cost of reactive power generation, the cost of an SVC is much lower than that of a rotating machine of the same capacity. Although the SVC's response time is much faster than its rotating machine counterpart, the final decision of adding reactive support into a system depends on the specific application and requirement.

Often, a voltage measurement at one bus is used as a control function for a second bus. Generators, synchronous condensers and SVC respond to control commands in a continuous manner. In many cases, these devices offer fast responses. The tap changing transformers; however, change in finite steps with significant time response delays.

In general, reactive power flow from a bus with a higher voltage magnitude to a bus with a lower voltage magnitude. Whereas, real or active power flow from a bus with a larger voltage angle to a bus with a smaller voltage angle. While an inductive reactive load tends to lower the voltage of the bus to which it is connected, a capacitive reactive load tries to raise the voltage of its bus. Consequently, the control of a system voltage profile can be made by adjusting the reactive output (within limits) of generators, synchronous condensers and SVCs. In addition, tap changing transformers are also used to control the voltage profile.

2.3 Definitions and Concepts

It has been said that a power system is either stable or unstable. This might be correct except that instability itself may be manifested in many

different forms depending upon the mode of operation and configuration of the system in time of trouble. Two types of stability of major concern are transient stability and steady-state stability.

According to [12, p.1895], steady-state stability is defined as:

> A power system is steady-state stable for a particular steady-state operating condition if, following any small disturbance, it reaches a steady-state operating condition which is identical or close to the pre-disturbance operating condition.

where

> A small disturbance is a disturbance for which the equations that describe the dynamics of the power system may be linearized for the purpose of analysis.

In other words, steady-state stability is the ability of synchronous machines to remain in synchronism after small disturbance. Of course, these small disturbances cannot cause loss of synchronism unless the system is operating near its steady-state stability limit. If this is the case, the system is in the state of angular instability. As a remainder, operating near the steady-state stability limit does not necessarily implies no voltage support or low system voltages. An example would be a highly compensated system.

In a recent IEEE activities [13, p.2], the voltage control problem is defined as:

Voltage stability is the ability of a system to maintain voltage so that when load admittance is increased, load power will increase, and so that both power and voltage are controlled.

Voltage collapse is the process by which voltage instability leads to loss of voltage in a significant part of the system. (voltage may be lost because of "angle instability" as well, and sometimes only a careful post-incident analysis can discover the primary cause.

Voltage security is the ability of a system, not only to operate stably, but also to remain stable (as far as the maintenance of system voltage is concerned) following any reasonably credible contingency or adverse system change.

When a rapid voltage drop occurs (because of a disturbance, an increase in load or change in system configuration) and all the control/corrective measures are exhausted, a power system is considered to be insecure and declared to be in the state of voltage instability. If voltages continue to deteriorate, voltage collapse or steady-state angular instability may occur. In the next section, a 2-bus example is used to illustrate the above concepts.

2.4 The 2-Bus Example

In order to establish a basic understanding of voltage instability and angular instability, a 2-bus system was selected. Although a normal size power system involves hundred of buses, the principles discussed remain valid for larger systems.

An extreme or unrealistic case of angle instability is the "pure angular instability." Figure 2.1 shows the configuration when a synchronous generator is connected to an infinite bus through a pure reactance, X.

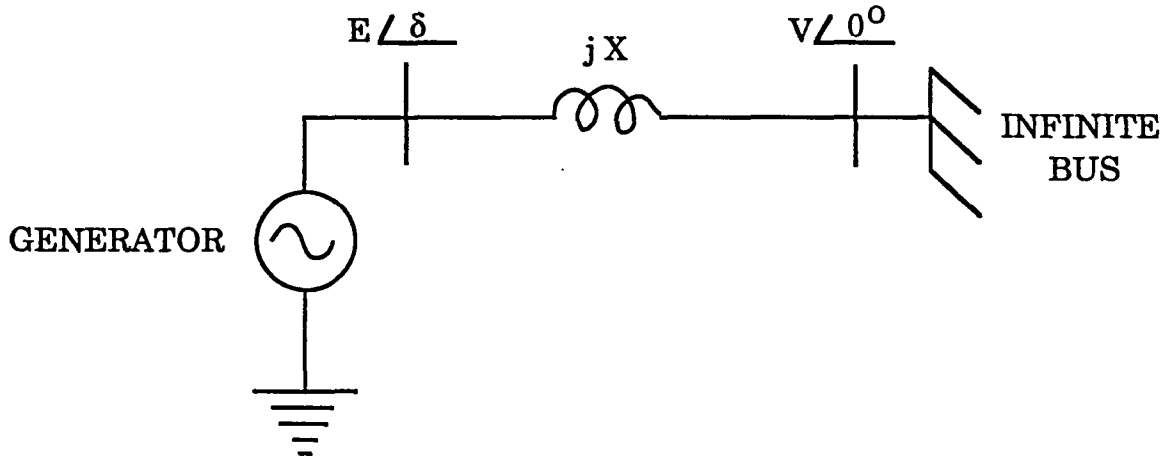

Figure 2.1: 2-bus system with infinite bus

Because no power is lost in the pure reactance, the electric output of the generator is equal to the electric input to the system. A power-angle curve is used to show how the power transmitted from the generator depends upon the

phase angle difference, δ, between the generator voltage, E and the infinite bus voltage, V. The equation that governs this curve is :

$$P = \frac{E\ V}{X} \sin \delta \qquad (2.1)$$

Assuming the load angle is 0° and the magnitudes of E and V are 1.1 p.u. and 1.0 p.u. respectively, the corresponding power-angle curve with X=1.0 p.u. is given in Figure 2.2. When δ is less than 90° the system is considered to be stable, since the real power transfer increases as the angle δ increases. On the other hand, an increase of δ beyond 90° causes a decrease in real power transfer to the load. When this happens, synchronism is lost and angular instability is encountered. In other words, the steady-state limit is reached when δ = 90°, which corresponds to the maximum power that can be transferred across the system [14,15].

The phenomenon of steady-state voltage instability in transmission networks can be demonstrated by considering the case of a "pure voltage instability", which occurs in the 2-bus system given in Figure 2.3. In this diagram, a load is connected to an infinite source through a reactance. Given a fixed load power factor or power factor angle where,

$$\text{load power factor} = \frac{P}{S} \qquad (2.2)$$

$$\text{power factor angle} = \varphi = \tan^{-1}\left(\frac{Q}{P}\right) \qquad (2.3)$$

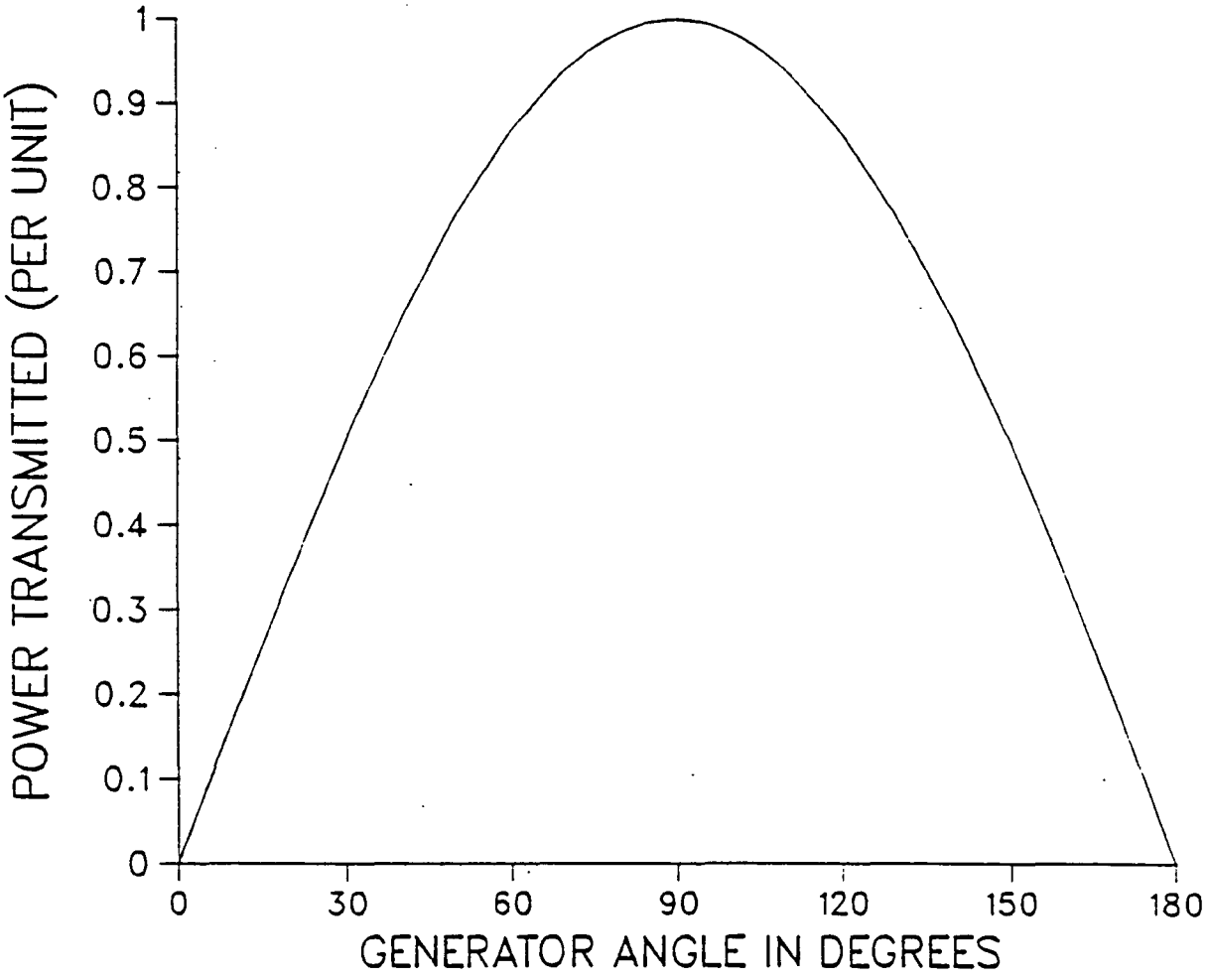

Figure 2.2: Power angle curve with infinite bus E = V = 1.0 p.u., X = 1.0 p.u.

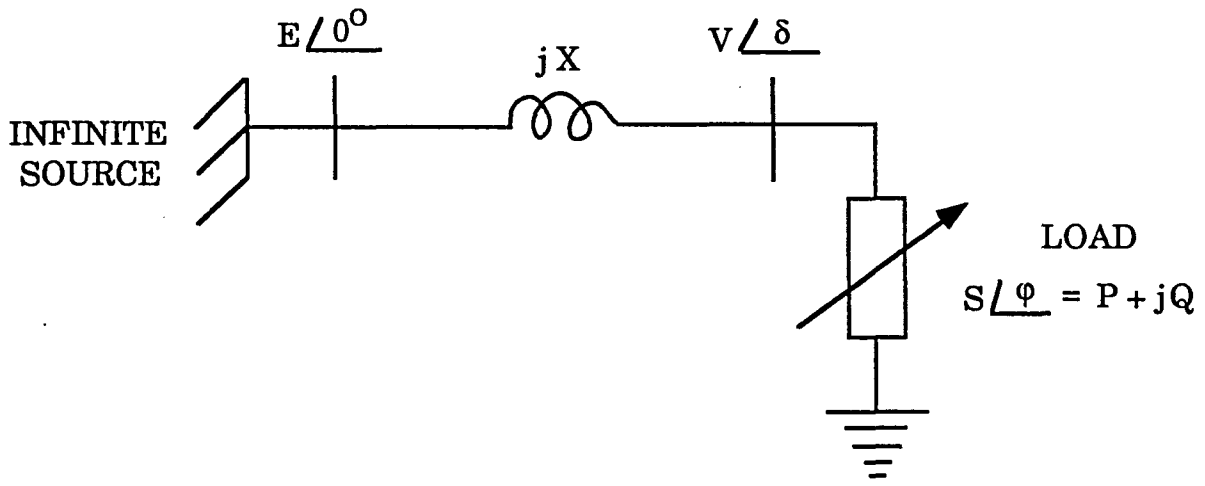

Figure 2.3: 2-bus system with infinite source

a P-V curve can be created following the configuration of Figure 2.3. This P-V curve given in Figure 2.4 depicts the overall operating state of a given system.

From Figure 2.4, the following comments can be made:

- From point A to B (the top half of the curve), the load voltage decreases as the load real power increases. Over this portion of curve, the slope is negative. This region is considered to be a stable operating region.

- Point B represents the critical point where the slope reverses its direction. The corresponding load level at this point represents the maximum power limit that theoretically can be delivered to the load.

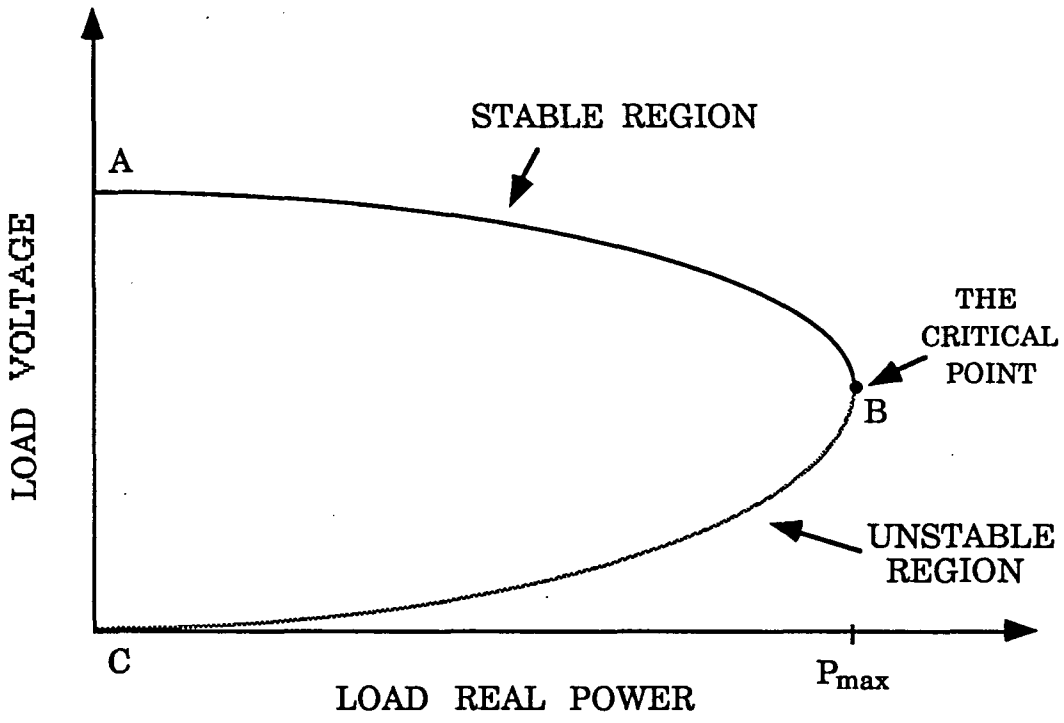

Figure 2.4: Illustration of the stable and unstable operation regions

- From point B to C (the lower half of the curve), the load voltage continues to decrease despite the effect of decreasing load. This region, having a positive slope, is considered to be an unstable operating region. Theoretically, no system should operating in this region since the control of voltage is lost.

In summary, there exists a critical point beyond which real power cannot be transmitted for a given load power factor. This is the steady-state voltage stability limit and the bus voltage corresponding to this limit value is the critical

voltage at that bus. Moreover, there are two operating points both mathematically valid for each real power level. One is a high voltage operating point or the stable operating point. The other is a low voltage operating point or the unstable operating point.

At this point, we have presented the information that is embedded in a P-V curve at a fixed load power factor. The next question is "What kind of conclusion can we drawn if the load power factor is being varied ?" Figure 2.5 displays the overall picture when the power factor angle of the load is varied. As the power factor angle increases or the power factor becomes more leading, one discovers that the critical point migrates to a higher voltage level with a greater real power transfer capability limit. This is equivalent to an increase of reactive (capacitive) compensation and a decrease of reactive (inductive) consumption to the system. When a system is highly compensated, the identity of the critical point can be hidden easily, if one merely compares the current operating voltage magnitude with the permissible voltage operating limits. This echoes the point given in Chapter 1 under the section of "Technical and Numerical Difficulties" that the use of voltage magnitude as a means to detect voltage instability is not sufficient for all operating conditions.

2.5 Additional Remarks

The above concepts are by no means the underlining principles behind steady-state voltage stability. In actual power systems, the region for stable and unstable operating conditions as well as the location of the critical point are not

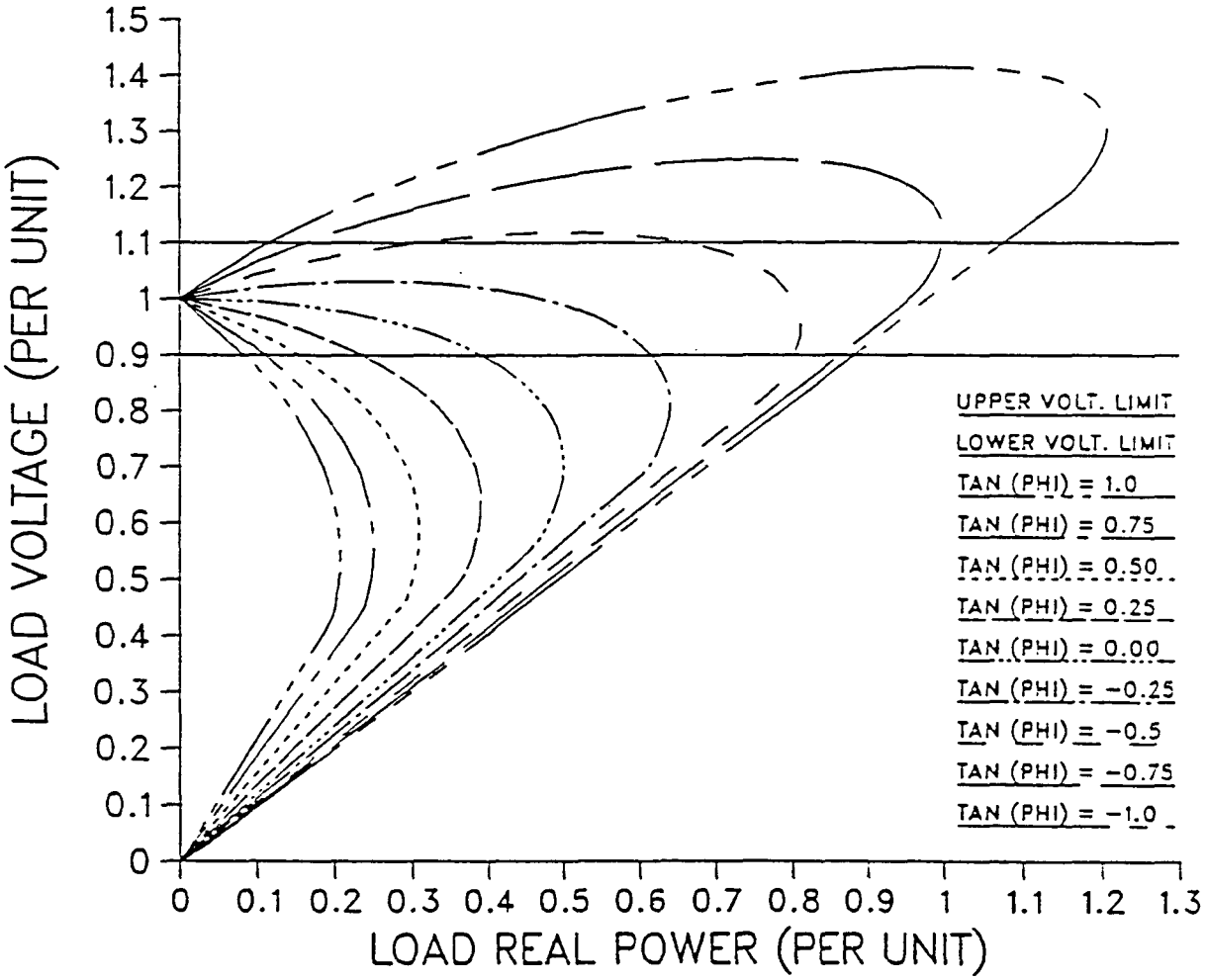

Figure 2.5: Collection of P-V curves with varying power factor angle φ (PHI)

so well-defined as they are in a 2-bus system. By taking into consideration the dynamical aspects of the power system and load modelling, researchers have reported cases of oscillation before voltage collapse [16]; stable operation in the unstable portion of the P-V curve; unstable operating condition in stable operating region. All these studies imply that the problem of voltage instability is far more complex than one can readily anticipate and more research is needed before the problem of voltage instability is understood fully.

2.6 The Direct Method

To understand why the ordinary power flow program fails to provide a solution at the critical point, the state of the Jacobian of the Newton-Raphson method is examined. Using the case of unity load power factor with the magnitude of the generator voltage $E=1.0\angle 0^0$ p.u., the determinant, J, is captured at the maximum load level, P=0.5 p.u. Details of the calculations of this Jacobian matrix is given in Appendix A for reference.

$$J = \begin{bmatrix} \frac{\partial P}{\partial \delta} & \frac{\partial P}{\partial V} \\ \frac{\partial Q}{\partial \delta} & \frac{\partial Q}{\partial V} \end{bmatrix} = \begin{bmatrix} \frac{-1}{2} & \frac{1}{\sqrt{2}} \\ \frac{1}{2} & \frac{-1}{\sqrt{2}} \end{bmatrix} \qquad (2.4)$$

The determinant of this Jacobian matrix is given by:

$$\det(J) = \frac{\partial P}{\partial \delta}\cdot\frac{\partial Q}{\partial V} - \frac{\partial Q}{\partial \delta}\cdot\frac{\partial P}{\partial V} = 0 \qquad (2.5)$$

It is this singular condition that creates the numerical barrier in the power flow program and prohibits the calculation of the critical point. In reality, the Newton-Raphson solution starts to diverge before the load level approaches its maximum limit.

Instead of making an approximation to the critical point when the solution starts to diverge, Alvarado [5] and Ajjarapu [4] suggest a direct method to locate the critical point in an exact manner. Basically, the direct method finds a power flow solution when the determinant of Jacobian matrix is singular. Since the concept in [4] is similar to the continuation power flow method described in the next chapter, the following review is provided.

Let $\mathbf{y} = [\, y_1\, y_2 \ldots\, y_n \,]^T$, $\mathbf{Z} = [\, z_1\, z_2 \ldots\, z_n \,]^T$, $\mathbf{X} = [\, \mathbf{y}\ \lambda\ \mathbf{Z} \,]^T$ where $\mathbf{y}$ is the state vector and λ is a parameter to be varied. If $X_0^T = [\, \mathbf{y}_0, \lambda_0, \mathbf{Z}_0 \,]$ is the solution to the following equations:

$$g(\mathbf{y}, \lambda) = 0 \qquad (2.6)$$

$$z_k - 1 = 0 \qquad (2.7)$$

$$g_y(\mathbf{y}, \lambda)\,\mathbf{Z} = 0 \qquad (2.8)$$

for k being a fixed index $1 \le k \le n$, then the (x_0, λ_0) is a critical point of the power flow equation $g(\mathbf{y}, \lambda) = 0$. Equation 2.8 establishes the singularity of the Jacobian and equation 2.7 ensures the vector $\mathbf{Z}$ is nonzero. Although the size of the equations to be solved is doubled by adding equation 2.8, the direct method need not be invoked until the operating point is sufficiently close to the critical point. This provides a powerful tool to locate the critical point when necessary.

The direct method avoids the problem of singularity by augmenting the original set of system equation with some appropriate vectors or equations. However, it is not always necessary to locate the critical point in a precise manner. The method about to discussed, not only approximates the critical point in an acceptable level, but also extends the capability of the ordinary power flow through a continuation technique. Moreover, the Jacobian remains well-conditioned throughout the entire continuation process.

3 THE PRINCIPLES OF CONTINUATION POWER FLOW

3.1 Introduction

The continuation method is a mathematical path-following methodology used for solving systems of linear and nonlinear equations [17]. In the literature, this method is also known as the imbedding, parametric programming, parameter variation, capacity or homotopy methods. Within the category of continuation methods, there are a variety of techniques or algorithms. However, the basic idea behind these techniques is to parameterize the problem in such a way that the solution can be found easily. The result of the continuation process is the solution trajectory as a function of the continuation parameter over its range of variation. A series of papers authored by Galiana, et. al. [18,19,20] reported the use of homotopy method to the optimal scheduling, planning and secure-economic dispatch problems.

Because the continuation method is a path-following method, it can track a solution branch around a turning or branch point without difficulty. This makes the continuation method particularly attractive to the application of approximating the critical point in the steady-state voltage instability problem.

The continuation power flow (CPF) [21] developed at Iowa State University is designed to capture this path-following feature using a predictor-corrector scheme with a locally parameterized technique to trace the power flow

solution path. In the following sections, the salient points of the continuation power flow are presented.

3.2 Local Parameterization

In the study of nonlinear phenomena, the term "branch" is often encountered. Basically, a branch is a curve consists of points, joined together in n+1 dimensional space, that are solutions to nonlinear functions,

$$\mathbf{F}(\mathbf{x},\lambda) = \mathbf{0} \tag{3.1}$$

By introducing a control parameter, λ, into the original system of nonlinear function, $\mathbf{F}(\mathbf{x}) = \mathbf{0}$, it is quite possible to identify each solution on the branch in a mathematical way. This process is called parameterization [22]. However, not every (or portion of a) branch can be parameterized by any arbitrary parameter.

Imagine a ship is located in the middle of a river which sails from north to south. We further assume a tug-boat is hired to pull this ship. If parameterization corresponds to the different directions in which the ship can be pulled, pulling the ship directly towards the west or the east is not recommended. Logically, the tug-boat shall pull the ship towards the south along the river. When the river bends towards the west, the tug-boat shall pull the ship in the same direction to avoid hitting the bank. In this situation, a change in direction or parameterization is necessary.

Similarly, in the local parameterization technique, all the state variables x_i and the control parameter, λ, are possible candidates to the continuation parameter. The choice of such parameter is locally determined at each continuation step.

3.3 Formulation

To implement the locally parameterized continuation technique to the power flow problem, a load (control) parameter, λ, is incorporated into the power flow equations:

$$0 = P_{Gi} - P_{Li} - P_{Ti} \tag{3.2}$$

$$0 = Q_{Gi} - Q_{Li} - Q_{Ti} \tag{3.3}$$

With slight modifications, the reformulated power flow equations or the continuation power flow equations of a n-bus system can be expressed as:

$$0 = P_{Gio}(1+\lambda k_{Gi}) - [P_{Lio} + \lambda(k_{Li} \cdot S_c \cdot \cos\psi_i)] - P_{Ti} \tag{3.4}$$

$$0 = Q_{Gio} - [Q_{Lio} + \lambda(k_{Li} \cdot S_c \cdot \sin\psi_i)] - Q_{Ti} \tag{3.5}$$

where

P_{Gio}, Q_{Gio} = original generation at bus i

P_{Ti}, Q_{Ti} = injection at bus i

P_{Lio}, Q_{Lio} = original real and reactive load at bus i

k_{Li} = load change multiplier at bus i as λ changes

k_{Gi} = constant for the rate of change in generation at bus i

S_c = a quantity for proper scaling of λ

ψ_i = power factor angle at bus i

This modification is applied to bus i through n except the slack bus. In the following discussion, the system of power flow equations will be written as

$$\mathbf{F}(\delta,\mathbf{V},\lambda) = 0 \ , \ 0 \le \lambda \le \lambda_{\text{critical}} \tag{3.6}$$

where δ, $\mathbf{V}$, λ represent the set of all bus angles, bus voltage magnitudes, load parameter respectively. $\lambda_{\text{critical}}$ is the load parameter value where the corresponding load level reaches the maximum limit.

To start the continuation power flow program, it is necessary to obtain two pieces of information; namely, a base case solution corresponds to $\lambda = 0$ and a search direction for the coming continuation process. It is no surprise that the load parameter is chosen as the first continuation parameter; since the the voltage magnitude and bus angle will experience minimal changes at the first incremental change of load level. Once the initial solution and the search direction (i.e. the tangent vector) are obtained, a predictor-corrector scheme is introduced as the path-following vehicle to find the subsequent solutions as λ increases along the power flow solution trajectory.

3.4 The Predictor-Corrector Scheme

The vehicle that performs the path-following is the predictor-corrector scheme (PCS). As a matter of fact, the predictor uses the calculated tangent vector from the previous step and predicts where the next possible solution will be within a specified step-size. In many cases, the predicted solution may deviate from the actual path. Under such conditions, it is necessary to correct the predicted solution so that the new solution would fall onto the solution path trajectory. Figure 3.1 illustrates the PCS on a voltage verses load parameter curve.

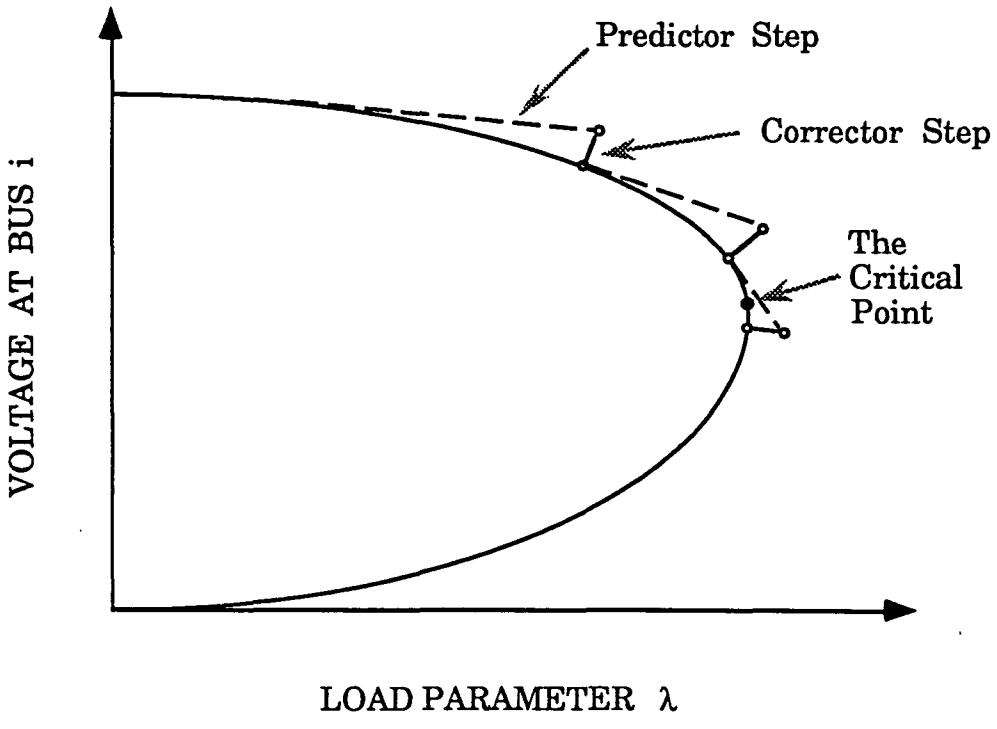

Figure 3.1: Illustration of the predictor-corrector scheme

Assume the i-th continuation step is being processed with a particular value of λ. A new solution is predicted by taking a predetermined step size in the direction tangent to the current operating point in the system. Mathematically, this is accomplished by taking the derivative on both sides of the power flow equations and set them to zero. However, the Jacobian has been augmented by an extra column vector $\mathbf{F}_\lambda$, but the number of power flow equations remains unchanged.

$$\begin{bmatrix} \mathbf{F}_\delta & \mathbf{F}_V & \mathbf{F}_\lambda \end{bmatrix} \begin{bmatrix} d\delta \\ dV \\ d\lambda \end{bmatrix} = 0 \qquad (3.7)$$

As a result, there are n+1 unknowns with n number of equations. In order to solve this set of equation, the following modification is necessary.

$$\begin{bmatrix} \mathbf{F}_\delta & \mathbf{F}_V & \mathbf{F}_\lambda \\ - - & - - & - - \\ & e_j & \end{bmatrix} \begin{bmatrix} \\ \mathbf{h} \\ \\ \end{bmatrix} = \begin{bmatrix} 0 \\ -- \\ \pm 1 \end{bmatrix}, \quad \mathbf{h} = \begin{bmatrix} d\delta \\ dV \\ d\lambda \end{bmatrix} \qquad (3.8)$$

An appropriately dimensioned unit row vector, e_j, is inserted with all elements equals to zero except the j-th element which has a value of one. This makes the enlarged system non-singular. Meanwhile, the choice of h_j which contains a value of either +1 or -1 will depend on how the j-th state variable is changing in the course of path tracing. The choice of this j-th variable and the sign of h_j will be clarified later in the discussion. Once we are able to solve for the tangent vector, **h**, at the current operating point, the predictor step is then modified by the following update:

$$\begin{bmatrix} \hat{\delta} \\ \hat{V} \\ \hat{\lambda} \end{bmatrix} = \begin{bmatrix} \delta \\ V \\ \lambda \end{bmatrix} + \alpha \begin{bmatrix} d\delta \\ dV \\ d\lambda \end{bmatrix} \tag{3.9}$$

where " ^ " denotes the newly predicted state variables for an increase of load in λ and " α " is the predefined step size.

For the corrector process, the original set of power flow equations is augmented by a parameterizing equation that specifies the continuation parameter being used. This parameter may be a bus voltage magnitude, a bus angle or the load parameter λ.

$$\begin{bmatrix} F(x) \\ x_j - \xi \end{bmatrix} = \begin{bmatrix} 0 \\ \end{bmatrix} \quad , \quad x = \begin{bmatrix} \delta \\ V \\ \lambda \end{bmatrix} \tag{3.10}$$

The choice of ξ comes from the predicted value of x_j. The index j is equivalent to the one used in the predictor step. This state variable x_j is the current continuation parameter. In the predictor step, the differential change of this state variable, dx_j or h_j is assigned to ± 1; whereas in the corrector step, the value of x_j is known by choosing the same continuation parameter from the predictor step. With the appropriate index j and ξ being chosen, the above equation can be solved easily by modifying the Newton-Raphson power flow algorithm.

3.5 Evaluation of the Continuation Parameter

The way to choose the right continuation parameter is to select the largest element in magnitude from the tangent vector **h**. Using the tug-boat analogy, the largest tangent vector element is similar to the concept of the direction in which the ship shall be pulled to cover the largest possible distance within a given step size.

Therefore, the subsequent continuation parameters are evaluated by

$$x_j : | h_j | = \max \{ | h_1 |, \ldots, | h_m | \} \tag{3.11}$$

at each successive continuation step where **h** is the tangent vector with a dimension of $m = 2n_{PQ} + n_{PV} + 1$. Here, n_{PQ} and n_{PV} are the number of PQ and PV buses respectively in a given power system. The index j corresponds to the largest element in the tangent vector **h**. This selected x_j state variable then

becomes the continuation parameter for next advancement. In addition, one should take note of the sign that belongs to the selected variable. This way, the proper value of +1 or -1 can be assigned to h_j in the next tangent calculation. A flow chart of the continuation power flow is displayed in Figure 3.2 as an outline of the overall process.

3.6 Determination of the Critical Point and the Weak Buses

Up to this point, the stopping criterion for the continuation power flow and the detection of the critical point have not been discussed. If the critical point corresponds to the maximum real load level of a given power system, the $d\lambda$ tangent component at this level should be zero. When the continuation process goes beyond the critical point, the $d\lambda$ tangent component becomes negative. Therefore, a test of the $d\lambda$ after each calculation of the tangent component determines whether or not the critical point has been passed.

As a preventive measure, it is of extreme interest to the system planners to identify buses that are most prone to voltage collapse. In this context, the concept of weak buses is introduced. In this research, a weak bus is defined as one that has a relative large ratio of differential change in voltage to differential change in system load, dV / dP_{TOTAL} . With this treatment, the effect of load increase at one bus to the surrounding buses will be taken into account. Systemwise, this gives the most accurate identification of the weak buses that are effective for remedial actions

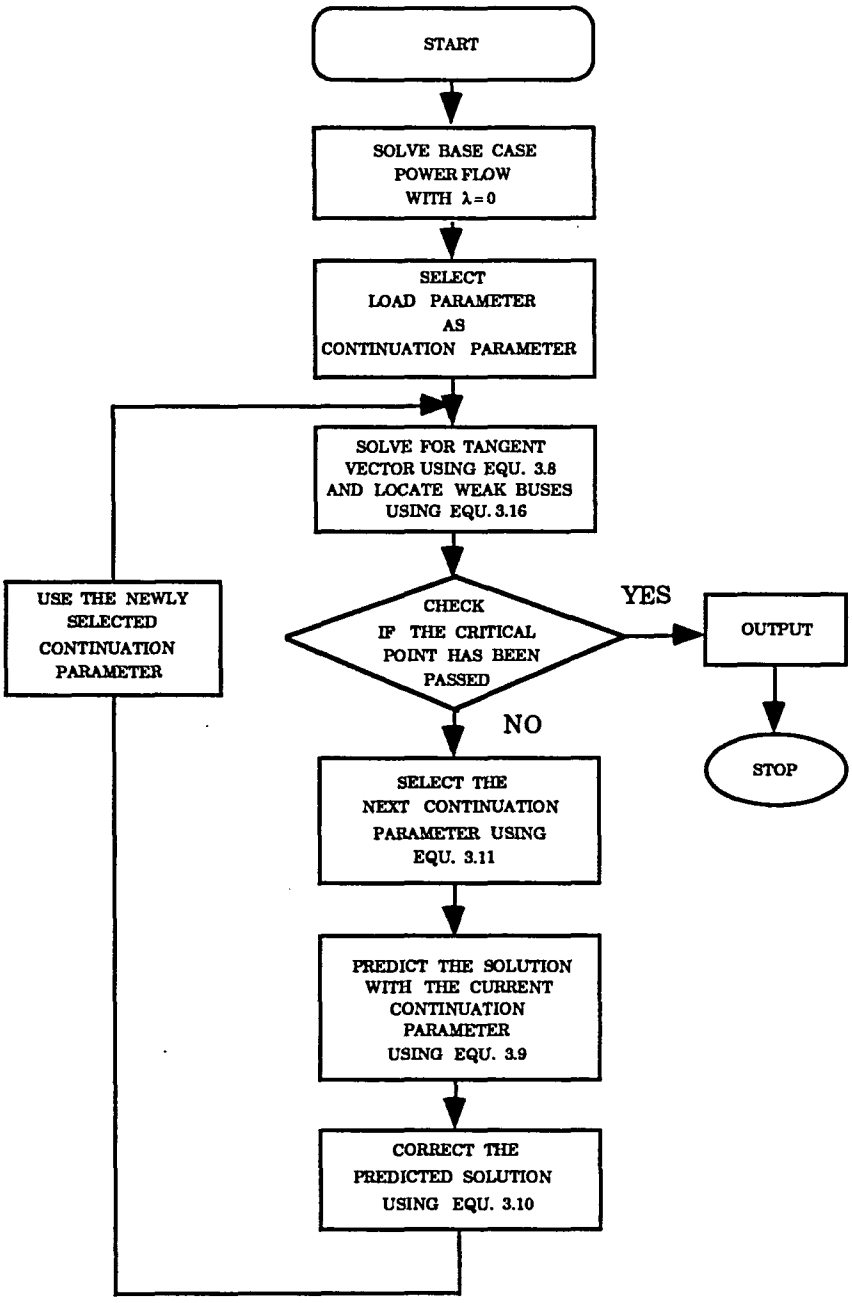

Figure 3.2: Flow chart of the continuation power flow

Since the tangent vector describes the trajectory of the various state variables at the corrected solution point, the information that describes how a differential change in the state variables responds to a differential change in the system load configuration is inherently available.

A close look at the reformulated power flow equations reveals that the differential change in real system load can be obtained as follows:

$$P_{Li} = P_{Lio} + \lambda \, (k_{Li} \cdot S_c \cdot \cos \psi_i) \tag{3.12}$$

$$P_{TOTAL} = \sum_{i=2}^{n} P_{Li} = \sum_{i=2}^{n} P_{Lio} + \lambda \, (k_{Li} \cdot S_c \cdot \cos \psi_i) \tag{3.13}$$

$$dP_{TOTAL} = \sum_{i=2}^{n} dP_{Li} = [\, S_c \cdot \sum_{i=2}^{n} k_{Li} \cdot \cos \psi_i \,] \cdot d\lambda$$

$$= R \cdot d\lambda \tag{3.14}$$

Following the discussion on weak buses, the mechanism of finding the weakest bus, m, will be

$$\text{bus } m = \left| \frac{dV_m}{dP_{TOTAL}} \right| = \left| \frac{dV_m}{R d\lambda} \right| \tag{3.15}$$

where

$$\left| \frac{dV_m}{R d\lambda} \right| = \max \left\{ \left| \frac{dV_2}{R d\lambda} \right| , \ldots , \left| \frac{dV_n}{R d\lambda} \right| \right\} \tag{3.16}$$

and n is the total number of buses in the system. Since the denominator, $R \cdot d\lambda$, is common to all elements, the weakest bus at a particular load level can be identified by searching the bus that has the largest $|dv|$ component in the calculated tangent vector.

$$| dV_m | = \max \left\{ | dV_2 | , \ldots , | dV_n | \right\} \tag{3.17}$$

To obtain the voltage stability index, one calculates the inverse of the rate of change of voltage write respect to the total system load of the weakest bus k at each load increment:

$$| dP_{TOTAL} / V_k | \tag{3.18}$$

the index should approach zero as the operating point becomes closer to the critical point.

In summary, the CPF method is a path-following methodology. To apply this method, the power flow equations are parameterized with a load parameter, λ. Then, a PCS is adopted as a vehicle to allow the movement along the solution path to the power flow equations. The driving force behind the CPF is the locally parameterization technique that generates a continuation parameter at each load level. It is the use of this continuation parameter that enables the CPF to overcome the numerical barrier of ill-conditioning at or near the critical point. It is important to point out that the continuation parameter at each load level is

not restricted to the load parmeter but rather to the voltage and angle of all buses except the slack bus.

At each load level, a tangent vector is calculated in the predictor step. Information from previous continuation parameter is used to assign a non-zero value to an appropriate tangent vector element. This latter vector augments the Jacobian and provides for the non-singular Jacobian matrix at the critical point. The same piece of information from previous continuation parameter is again being used to augment the system in the corrector stage.

The tangent vector is a source of sensitivity information since the tangent vector calculated at each load level gives the differential change in bus voltage magnitudes (dV), bus angle ($d\delta$) for a given differential change in load parameter ($d\lambda$). By comparing the sensitivity at each bus to a given differential change in system load, the buses that are susceptible to voltage collapse can be identified.

One of the objectives in this reseach is to obtain a methodology that calculates the maximum real power transfer with respect to voltage collapse through continuation power flow. This is equivalent to an optimization problem with an objective to maximize a given function subject to equality and inequality constaints. To pave the path for the proposed methodology, the optimal power flow that is designed to solve similar problem is reviewed in the next chapter.

4 THE OPTIMAL POWER FLOW

4.1 Introduction

In general, optimization problems involve finding the maximum or minimum of an objective function by adjusting the control variables. The result is the value of the objective function and the corresponding set of state variables that ensure the given constraints are satisfied.

An optimal power flow (OPF) is a power flow that minimizes a user specified objective function while recognizing the limitations on power system equipments and operation constraints (i.e. LTC tap limits, reactive power generation limits, line flow limits and bus voltage limits etc.).

Although economics dispatch (ED) can be regarded as the predecessor of OPF, the functionalities of the two are rather different. In principle, ED allocates the required real power load demand among available generation units in such a way that the operation cost is minimized. The OPF, on the other hand, is more general and capable of optimizing the performance of the entire power system network. When total fuel cost is minimized , the OPF is basically performing an economic dispatch. Furthermore, the OPF provides information such as the reactive power output of each generator, LTCs' tap setting.

The application of optimization to the a.c. power flow problem was first formulated in 1961 by Carpentier [23] of Electricité de France. Since then,

methods with various techniques ranging from linear to nonlinear programming (based on Kuhn-Tucker conditions, penalty functions, Newton's Method) as well as their derivatives have been proposed and implemented.

In 1968, Dommel and Tinney [24] introduced a reduced gradient steepest-decent algorithm with exterior penalty functions. A method centered around the solution of power flow problem by Newton's Method. Lagrangian multipliers were used to associate power flow equation to the objective function and penalty function to handle inequality constraints.

Though the drawbacks of this approach involved the slow convergence with the steepest descent direction and the ill-conditioning resulting from the penalty function, this paper prepared by Dommel and Tinney became a classical example for the study of OPF problem thereafter.

4.2 Applications of the Optimal Power Flow

Because the OPF problem considers both the security and economic aspects of a power system, the OPF has many applications in the power system planning, control operations and operations planning. In the operations and control environments, the OPF is used as a decision-making tool taking into consideration of the economic impact because of thermal, voltage and stability constraints. Figure 4.1 lists some of the applications of the OPF in power systems.

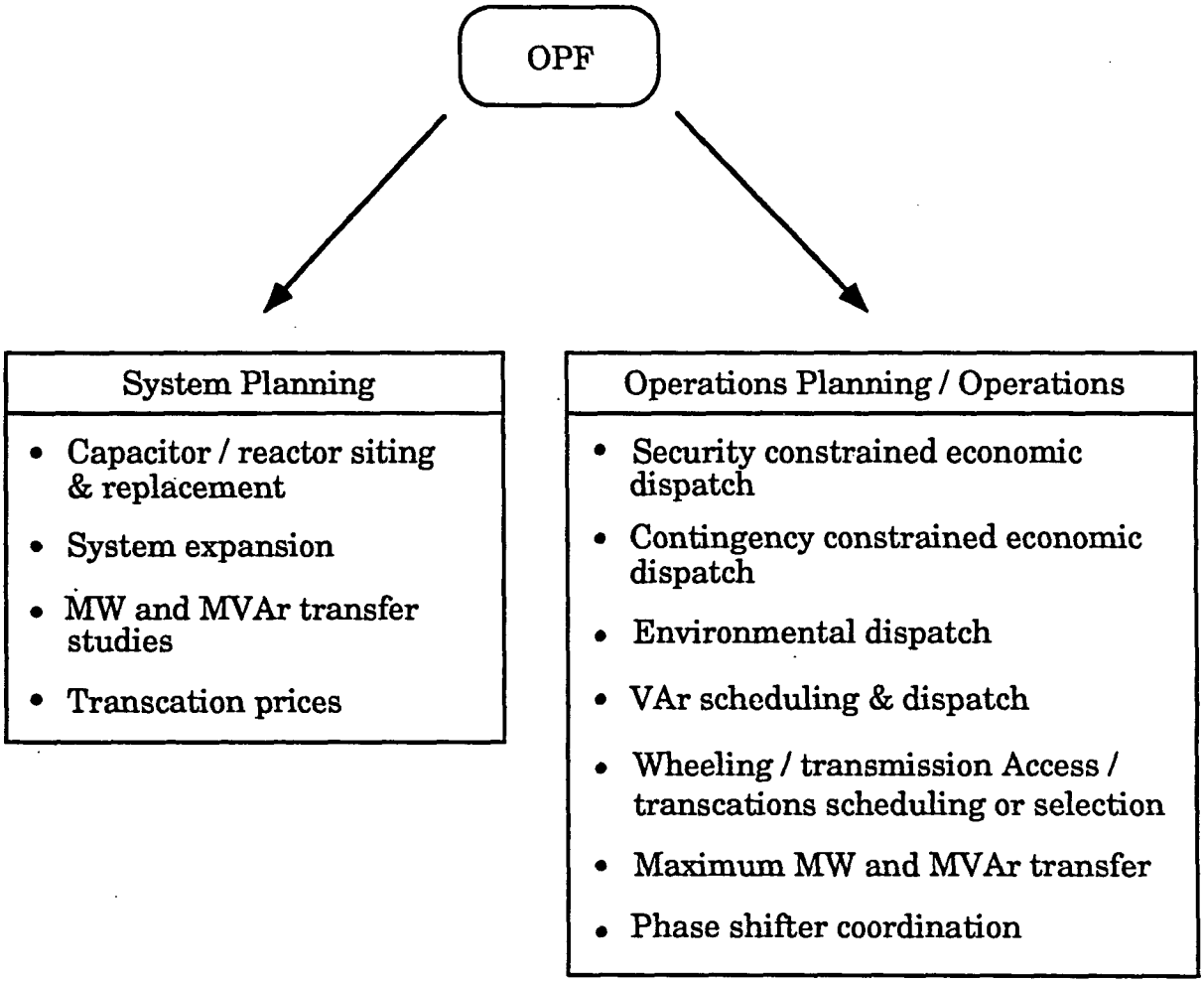

Figure 4.1: Applications of the optimal power flow in power systems [25]

Over the last decade, the linear programming (LP) method has emerged as a dominant optimization method for solving on-line OPF problems. However, the development of fast and reliable on-line OPF that considers nonlinear security constraints is still a research topic of interest.

4.3 Formulation of the Optimal Power Flow

The OPF problem is nonlinear because the power flow equations are nonlinear functions of voltage, angle, tap ratios and phase shifters. Furthermore, the objective function may be a nonlinear function of the same variables.

Consider the scalar objective function f to be a function of the control (independent) variable vector, **u** and the state (dependent) variable vector, **x**:

$$f = f(\mathbf{x},\mathbf{u}) \tag{4.1}$$

which will be minimized subject to the power flow equality constraints

$$\mathbf{g}(\mathbf{x},\mathbf{u}) = \mathbf{0} \tag{4.2}$$

and the functional inequality constraints such as line flow limits, generator reactive power limits

$$\mathbf{h}(\mathbf{x},\mathbf{u}) \leq \mathbf{0} \tag{4.3}$$

with inequality constraints on the control and state variable vectors such as voltage limits on generator buses and load buses respectively.

$$\mathbf{u}_{min} \leq \mathbf{u} \leq \mathbf{u}_{max} \tag{4.4}$$

$$\mathbf{x}_{min} \leq \mathbf{x} \leq \mathbf{x}_{max} \tag{4.5}$$

Therefore, the nonlinear constrained optimal power flow problem becomes

$$\min \; f(\mathbf{x},\mathbf{u}) \tag{4.6}$$

subject to

$$\mathbf{g}(\mathbf{x},\mathbf{u}) = \mathbf{0}$$

$$\mathbf{h}(\mathbf{x},\mathbf{u}) \leq \mathbf{0}$$

$$\mathbf{u}_{min} \leq \mathbf{u} \leq \mathbf{u}_{max}$$

$$\mathbf{x}_{min} \leq \mathbf{x} \leq \mathbf{x}_{max}$$

4.4 Types of Objective Function

In power system, the choice of objective function depends on the application of the result. Some common objectives include:

- minimization of the real(active) power transmission losses
- minimization of the cost of real power generation
- minimization of voltage deviation from a given system profile

- minimization of the cost of installing reactive power compensators
- maximization of the reactive margin

4.5 Some Techniques for Solving Optimal Power Flow

During the last three decades, numerous programming techniques had been applied to the OPF problem [26]. Among the techniques used by the engineers, analysts and utilities are

- Sequential (successive) linear programming method [27,28,29]
- Augmented Lagrangian method [30,31]
- Newton's method [32,33]
- Sequential quadratic programming [34]

In this research, an optimization package [35] using the sequential quadratic programming (SQP) method from the Numerical Algorithm Group (NAG) was adopted. A derivation of the SQP technique with equality constraints is given in Appendix C for interested reader.

In short, SQP tries to solve a sequence of simpler subproblems that quadratically converge to the solution of the original problem. In other words, the idea behind SQP is based on the sequential resolution of subproblems with an objective function. This objective function results from the approximation of the Lagrangian function of the OPF by a quadratic function and with constraints

obtained from the linearization of the nonlinear constraints of the original problem. By solving the quadratic programming subproblem, the direction of search is obtained.

Having established the background information, the next chapter is prepared to introduce a strategy that meet the objectives of this research. This strategy, which interfaces with the continuation power flow, identifies two specific schemes. First, a predictor-corrector optimization scheme is presented. Then, a relaxation scheme which improves the performance of the voltage stability index is suggested. Results from both schemes are compared and assessments are made to foster further insight.

5 AN OPTIMAL STRATEGY AGAINST VOLTAGE COLLAPSE

5.1 Introduction

The motivation behind this research came from two sources. One is the incentive to provide a preventive measure against voltage collapse using the weak bus information from the CPF (continuation power flow). The second incentive comes from the desire to increase the real power transfer capability through reactive power injection. Figure 5.1 reminds us how the change in

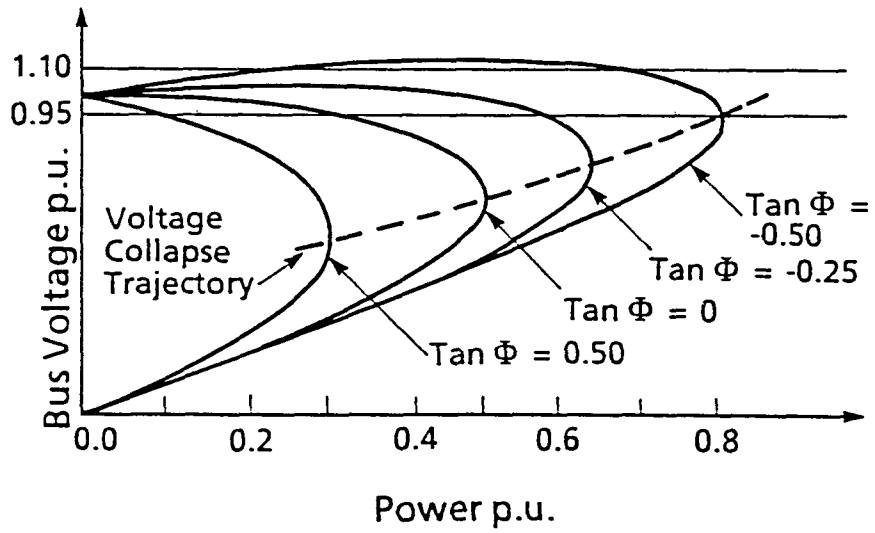

Figure 5.1: Shift of the critical point

power factor angle (Φ) because of capacitive reactive injection would lead to the improvement of real power transfer capability in a 2-bus system. Notice, the critical point does not disappear. It simply migrates along a trajectory as the tangent of the load power factor angle, tan Φ, becomes more and more leading.

5.2 Problem Statement

Since the CPF indicates the maximum load level that a system can handle for a given load increase scenario, the CPF may be used to increase the power transfer capability for a given system. This leads to following problem statement:

> Maximizes the real power transfer capability of a given system with minimum amount of shunt reactive power injection at selected weak buses via continuation power flow

This can be written as:

minimize [total VAr injection at selected weak buses]

subject to

(i) Continuation power flow equations
(ii) All bus voltages within specified operating limits
(iii) Allowable shunt VAr supply at each injection site

In mathematical form,

minimize

$$\sum_{j \in S_W} (q_{cj} + q_{rj})$$

subject to

$$P_{Gi}(\delta, \mathbf{V}, \lambda) - P_{Li}(\delta, \mathbf{V}, \lambda) - P_{Ti}(\delta, \mathbf{V}) = 0$$

$$Q_{Gi}(\delta, \mathbf{V}) - Q_{Li}(\delta, \mathbf{V}, \lambda) - Q_{Ti}(\delta, \mathbf{V}) - q_{ci} - q_{ri} = 0$$

$$\begin{array}{ccccccc} V_{i\,min} & \leq & V_i & \leq & V_{i\,max} & & i \in S_L \\ 0 & \leq & q_{cj} & \leq & q_{cjmax} & & j \in S_W \\ 0 & \leq & q_{rj} & \leq & q_{rjmax} & & j \in S_W \end{array} \qquad (5.1)$$

where

S_W = the set of selected weak load buses

S_L = the set of PQ load buses

V_i = voltage magnitude at bus i

q_{cj} = additional capacitive VAr at bus j

q_{rj} = additional inductive VAr at bus j

$\mathbf{V}$ = vector of bus voltages

δ = vector of bus angles

λ = load parameter

P_{Gi}, Q_{Gi} = active and reactive generation at bus i

P_{Li}, Q_{Li} = active and reactive load at bus i

P_{Ti}, Q_{Ti} = active and reactive injection at bus i

In this research, the shunt reactive power resources are treated as infinite so that the demand of reactive power support is always available to allow maximum real power transfer before voltage collapse.

At the programming level, the best place to implement the problem statement is to interface the CPF with an optimization routine after each corrector step. This approach is called the predictor-corrector optimization scheme (PCOS). Figure 5.2 illustrates this process with a P-V curve. The corresponding flow chart is also provided in Figure 5.3 for reference.

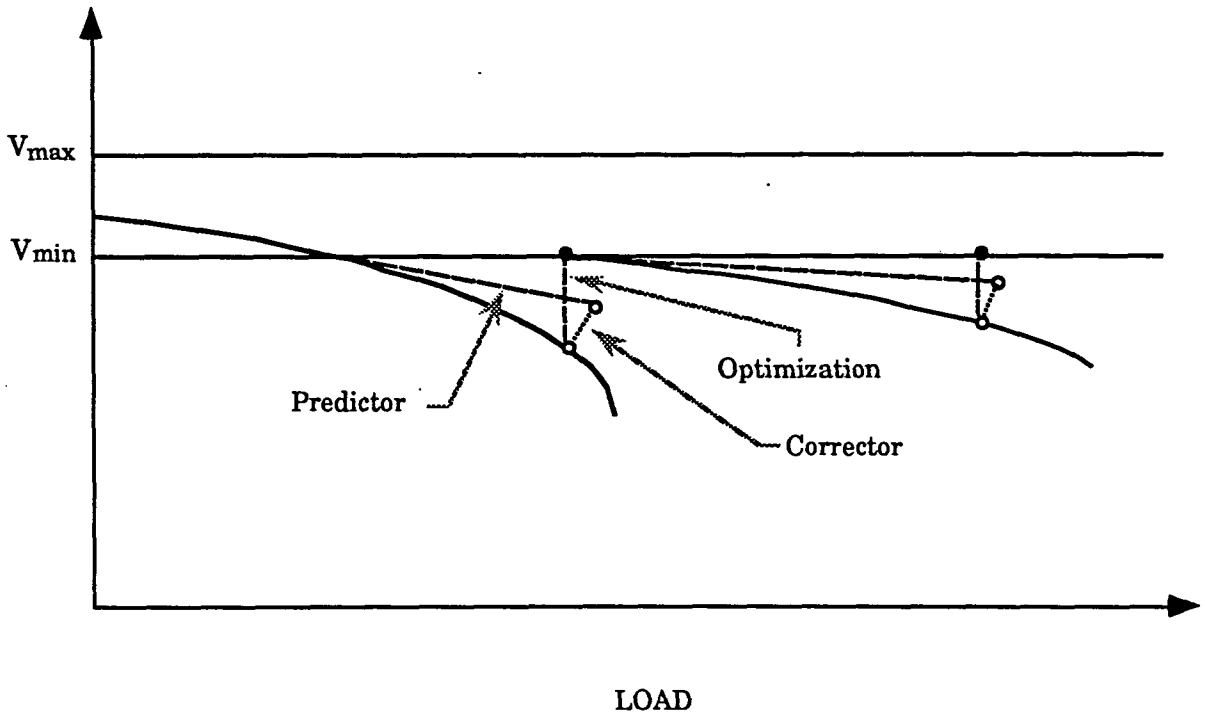

Figure 5.2: Illustration of the predictor-corrector optimization scheme

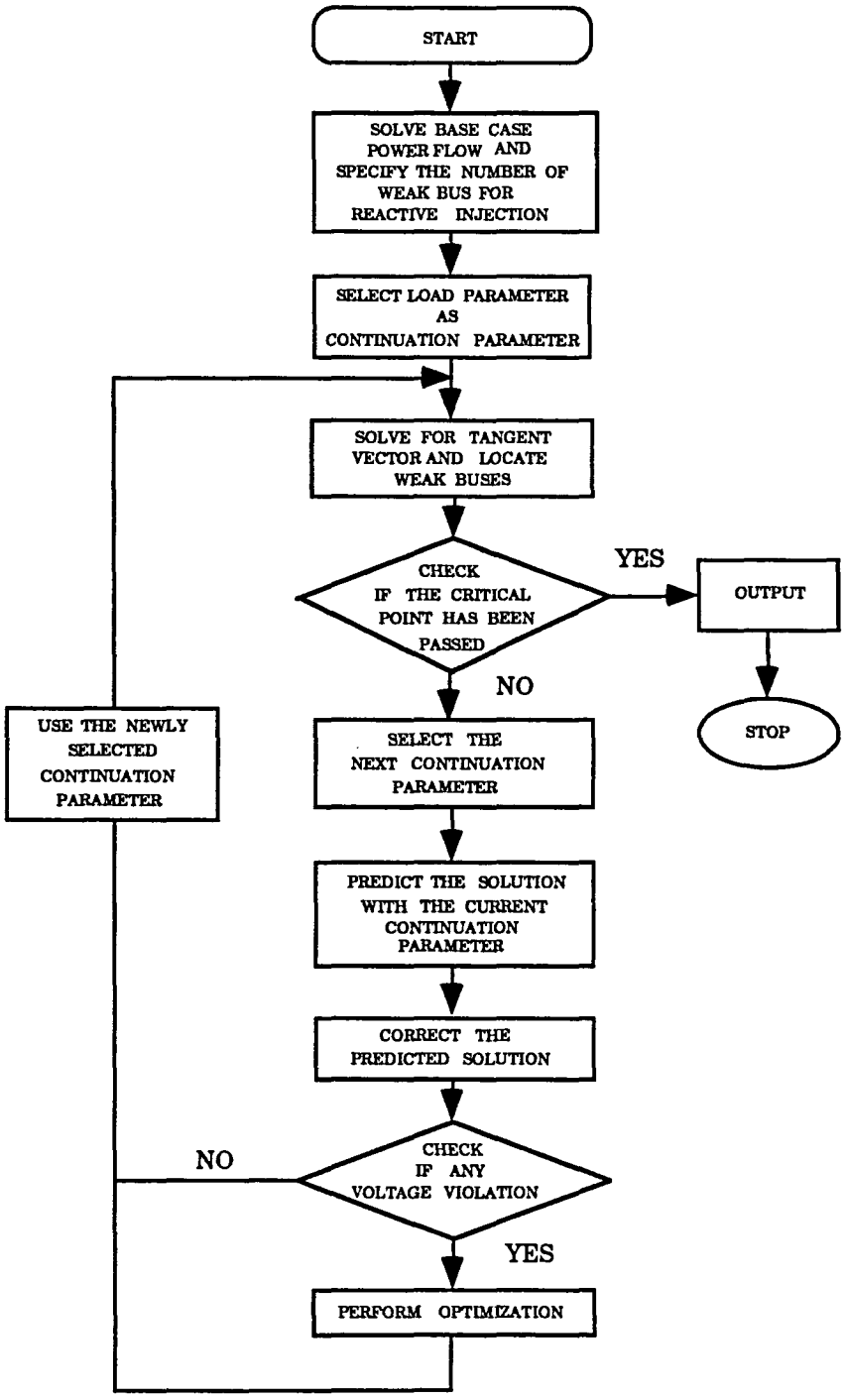

Figure 5.3: Flow chart of the predictor-corrector optimization scheme

Because of the reactive injection terms in the modified continuation power flow equations, a submatrix J5 is created to include the terms $\partial Q_i/\partial q_j$ where qj = $q_{cj} + q_{rj}$, $i \in S_L$ and $j \in S_W$. The dimension of J5 is dictated by the number of selected weak buses requested by the user. For example, a user may only interested in the top five weak buses that are most likely to cause voltage collapse at each load level for shunt reactive power injection. In addition to the size of the submatrix, buses that are considered to be "weak" vary from one load level to the next. For example in the New England 30-bus system, bus 21 may be the weakest bus at a particular load level. But for the next increment of load, bus 16 may replace bus 21 as the weakest bus in the system. This implies that the pattern of J5, which composes of 1 and 0, varies as load increases.

$$J = \left[\begin{array}{c|c|c} J1 & J2 & 0 \\ \hline J3 & J4 & J5 \end{array}\right] \qquad (5.2)$$

5.3 Application of the Predictor-Corrector Optimization Scheme

Before executing the original version of the CPF, the user is required to specify some key parameters:

(1) EST = estimated multiples of the based load level to voltage collapse
(2) λ_{DES} = desired load parameter value when voltage collapse occurs
(3) λ_{STEP} = specified step size for the load parameter
(4) V_{STEP} = specified step size for bus voltage
(5) δ_{STEP} = specified step size for bus angle

The EST and λ_{DES} are used as scaling parameters to the overall continuation process. Whereas, parameters (3) to (5) define the step size for the predictor step. Various levels of tolerance as well as permissible number of iterations are also required to establish stopping criteria.

To implement the PCOS, several systems were being tested. The data and the configuration of these systems are provided in Appendix D for references. The following tables (Tables 5.1 – 5.11) compare the results under the PCOS to that of the PCS (predictor-corrector scheme) from the original CPF. In addition, the corresponding voltage stability indices using the normalized $d\lambda$ as an indicator are listed. For all executions, the step size for λ, V, δ are set to

0.05, 0.03, 0.02 respectively. Furthermore, the upper and lower voltage operating limits imposed onto the PCOS are 1.10 and 0.95 p.u. respectively.

Four test systems are being used throughout this research. They include: 1) A 2-bus system that is simple enough to test new approaches; 2) An AEP 14-bus system that reflects the condition where the generation is far away from the load centers; 3) A 16-bus system that served as one of the initial test systems for CPF; 4) The New England 30-bus system that is commonly used in voltage stability research.

Table 5.1: PCS, PCOS results from the 2-bus system with EST=8.0, λ_{DES}=1.5

METHOD	MAXIMUM SYSTEM REAL POWER TRANSFER IN P.U.*	REACTIVE INJ. IN P.U. CAP. / IND.	WEAK LOAD BUS † LOCATIONS BEFORE VOLTAGE COLLAPSE	LOWEST BUS VOLT. IN P.U.
PCS	0.640	0.000 / 0.000	2	0.814
PCOS	0.794	-0.183 / 0.000	2	0.950

* INITIAL SYSTEM REAL POWER = 0.1 p.u.
† NUMBER OF WEAK LOAD BUSES FOR REACTIVE INJECTION = 1

With the PCOS, Tables 5.1 – 5.4 demonstrate that the maximum real power transfer for the 2, 14, 16, 30-bus system can be improved by injecting reactive power. For example, the maximum real power transfer of the 2-bus system increases from 0.64 to 0.794 p.u.; an increase of 0.154 p.u. with a total reactive (capacitive) injection of -0.183 p.u. Selected as the first test system, the 2-bus system is used to verify the approach of the PCOS. In Table 5.1, the

Table 5.2: PCS, PCOS results from the 14-bus system with EST=2.0, λ_{DES}=0.48

METHOD	MAXIMUM SYSTEM REAL POWER TRANSFER IN P.U.*	REACTIVE INJ. IN P.U. CAP. / IND.	WEAK BUS † LOCATIONS BEFORE VOLTAGE COLLAPSE	LOWEST BUS VOLT. IN P.U.
PCS	4.382	0.000 / 0.000	14,13,10,12,9	0.594
PCOS	9.444	-8.767 / 0.987	3,4,14,7,9	0.950

* INITIAL SYSTEM REAL POWER = 2.590 p.u.
† NUMBER OF WEAK BUSES FOR REACTIVE INJECTION = 5

registered maximum real power transfer before voltage collapse is 0.794 p.u. This compared comfortably with the value of 0.80 p.u. shown in Figure 5.1. At this load level, the critical point is resided at the specified 0.95 p.u. lower voltage limit. Also, the bus voltage is improved from 0.814 to 0.95 p.u. using the PCOS.

The next system under study is the AEP 14-bus system. According to Table 5.2., this system is capable of extending its real power transfer capability by 5.062 p.u. (9.444 – 4.382 p.u.). Later in the assessment section, experience gathered from this particular system is further discussed.

From Table 5.3 and 5.4, it is found that the maximum real power transfer of the 16-bus system improves from 5.241 to 9.298 p.u. This is accomplished by

Table 5.3: PCS, PCOS results from the 16-bus system with EST=2.0, λ_{DES}=0.48

METHOD	MAXIMUM SYSTEM REAL POWER TRANSFER IN P.U.*	REACTIVE INJ. IN P.U. CAP. / IND.	WEAK LOAD BUS † LOCATIONS BEFORE VOLTAGE COLLAPSE	LOWEST BUS VOLT. IN P.U.
PCS	5.241	0.000 / 0.000	16,15,2,4,6	0.635
PCOS	9.298	-4.529 / 0.000	16,15,4,2,6	0.950

* INITIAL SYSTEM REAL POWER = 4.250 p.u.
† NUMBER OF WEAK LOAD BUSES FOR REACTIVE INJECTION = 5

injecting -4.529 p.u. of shunt reactive support. The negative sign indicates that the reactive support is capacitive in nature. Similarly, in Table 5.4, -4.990 p.u. of shunt reactive support is required to improve the maximum real power transfer of the 30-bus system from 106.855 to 118.255 p.u. One of the characteristics of the PCOS is that all bus voltages are maintained at or above the user specified lower voltage limit. In this research, it is set to 0.95 p.u.

Table 5.4: PCS, PCOS results from the 30-bus system with EST=3.0, λ_{DES}=0.4

METHOD	MAXIMUM SYSTEM REAL POWER TRANSFER IN P.U.*	REACTIVE INJ. IN P.U. CAP. / IND.	WEAK LOAD BUS † LOCATIONS BEFORE VOLTAGE COLLAPSE	LOWEST BUS VOLT. IN P.U.
PCS	106.855	0.000 / 0.000	12,7,8,5,11	0.914
PCOS	118.255	-4.990 / 0.000	12,7,8,5,11	0.950

* INITIAL SYSTEM REAL POWER = 50.465 p.u.
† NUMBER OF WEAK LOAD BUSES FOR REACTIVE INJECTION = 5

Meanwhile, Tables 5.5 – 5.6 illustrate the performance of the voltage stability index in the 2-bus system under the PCS and PCOS respectively. Both indices decrease monotonically except the sudden change in sign (from positive to negative) which indicates the critical point has been passed.

Though the voltage stability index given in Table 5.7 maintains a decreasing trend as in the 2-bus system, a similar trend has not been recorded for the 14-bus system in Table 5.8 under the PCOS. In fact, the corresponding index fluctuates up and down until it turns negative which implies the critical point has been passed. Similar observations are recorded in Tables 5.10 and 5.12 for the 16, 30-bus systems respectively.

Table 5.5: Voltage stability index under PCS using the 2-bus system

SYSTEM REAL POWER TRANSFER IN P.U.	VOLTAGE STABILITY INDEX
0.1000	0.9090
0.2167	0.9084
0.3333	0.8955
0.4500	0.8587
0.5667	0.7271
0.6299	0.3685
0.6404	0.0110
0.6405	-0.6628

Table 5.6: Voltage stability index under PCOS using the 2-bus system

SYSTEM REAL POWER TRANSFER IN P.U.	VOLTAGE STABILITY INDEX
0.4500	0.8587
0.5900	0.6908
0.6387	0.6032
0.6809	0.5000
0.7223	0.3682
0.7415	0.2965
0.7565	0.2353
0.7682	0.1847
0.7774	0.1438
0.7844	0.1114
0.7899	0.0859
0.7942	0.0661
0.7948	-0.0021

Table 5.7: Voltage stability index under PCS using the 14-bus system

SYSTEM REAL POWER TRANSFER IN P.U.	VOLTAGE STABILITY INDEX
2.5900	0.4959
3.3994	0.3165
3.9390	0.2079
4.1140	0.1594
4.2363	0.1160
4.2810	0.0960
4.3163	0.0772
4.3625	0.0423
4.3817	0.0110
4.3829	-0.0036

Table 5.8: Voltage stability index under PCOS using the 14-bus system

SYSTEM REAL POWER TRANSFER IN P.U.	VOLTAGE STABILITY INDEX
8.4548	0.0772
8.5790	0.0703
8.6907	0.0641
8.7909	0.1978
9.0044	0.1665
9.1227	0.1843
9.2576	0.1708
9.3574	0.0198
9.4441	0.0146
9.4462	-0.0001

Table 5.9: Voltage stability index under PCS using the 16-bus system

SYSTEM REAL POWER TRANSFER IN P.U.	VOLTAGE STABILITY INDEX
4.2500	0.4947
4.6927	0.3977
4.8009	0.3640
4.8967	0.3284
5.0128	0.2741
5.1009	0.2189
5.1650	0.1634
5.2080	0.1085
5.2324	0.0549
5.2407	0.0033
5.2349	-0.0457

It is important to point out that the voltage stability index even under the PCS in the continuation power flow is subject to deviation caused by the change in generator status. From experience, the deviations are generally small in magnitude. Therefore, large degree of deviation that affects the performance of the voltage stability index is not anticipated.

Given the results under the PCOS in Tables 5.8, 10, 12 for the 14, 16, 30-bus systems, it is logical to examine the mechanics behind the PCOS that may affect the performance of the voltage stability index. In fact, the problem with the PCOS may be related to the flat tangent vector profile generated by the optimization process. As a result, changes in generator status that affect the performance of the voltage stability index become more obvious and influential.

Table 5.10: Voltage stability index under PCOS using the 16-bus system

SYSTEM REAL POWER TRANSFER IN P.U.	VOLTAGE STABILITY INDEX
8.3739	0.0869
8.5140	0.2222
8.6581	0.0662
8.8088	0.0547
8.9127	0.1739
8.9978	0.1626
9.0842	0.0339
9.1625	0.0272
9.1872	0.0258
9.2572	0.0197
9.2984	0.1231
9.3221	-0.0018

Table 5.11: Voltage stability index under PCS using the 30-bus system

SYSTEM REAL POWER TRANSFER IN P.U.	VOLTAGE STABILITY INDEX
50.465	0.1328
65.973	0.1293
74.544	0.1269
80.140	0.1230
85.585	0.1203
90.908	0.1174
98.298	0.0993
102.784	0.0924
106.855	0.0635
107.709	-0.0002

Table 5.12: Voltage stability index under PCOS using the 30-bus system

SYSTEM REAL POWER TRANSFER IN P.U.	VOLTAGE STABILITY INDEX
90.908	0.1174
109.063	0.0663
110.904	0.0087
111.950	0.0085
112.962	0.0083
113.940	0.0081
114.574	0.0080
115.279	0.0614
118.255	0.0578
119.556	-0.0020

Using the 30-bus system, the effect of increasing the specified number of injection buses to the real power transfer capability is studied. From Table 5.13, it has found that the real power transfer actually decreases as the number of injection buses increases. This can be explained as follows: as the number of injection sites increases, the voltage profile across the system will be improved. Correspondingly, the incident of voltage violations will reduce and the demand for reactive power support necessary to rectify the voltage violations will decrease also. As a result, the transfer of real power which is enhanced by the support of reactive power decreases. While referring to the 30-bus system, a typical PCOS output table is provided in Figure 5.4 for reference.

For further investigation, the same 30-bus system is used to follow the weak bus locations. With generators in PQ mode colored in blue and generators

Table 5.13: Effect of increasing the number of injection buses to real power transfer with EST=3.0, λ_{DES}=0.4 in the 30-bus system

SPECIFIED NUMBER OF INJECTION BUSES AT EACH LOAD LEVEL	MAXIMUM SYSTEM REAL POWER TRANSFER IN P.U.	TOTAL NUMBER OF CAPACITIVE INJECTION SITES	REQUIRED TOTAL CAPACITIVE INJECTION IN P.U.	IDENTIFIED WEAK BUSES FOR CAPACITIVE INJECTION BEFORE VOLTAGE COLLAPSE
1	125.757	3	-8.547	28
3	119.642	7	-5.616	12,7,5
5	118.255	10	-4.990	12,7,8,5,11
7	114.992	12	-3.085	21,15,24,16,12,14,13
9	112.509	14	-2.099	21,15,24,16,12,14,13,4,17

in PV mode colored in red, the results found in Table 5.14 are mapped onto Figure 5.5. From this figure, it is evident that weak buses migrate across the system as the real load level increases. Unfortunately, these weak bus locations cannot be predicted since the continuation method is associated with a path-dependent approach. Another observation is made when the system load increases, the number of generators that switch from PV to PQ mode increases.

Table 5.14: Shift of the weak buses' location at various system load level in the New England 30-bus system

SYSTEM REAL LOAD LEVEL IN P.U.	MULTIPLES OF THE SYSTEM REAL BASE LOAD	THE TOP THREE WEAKEST BUSES IN THE SYSTEM
50.465	1.000	15,27,17
77.357	1.533	8,7,15
95.949	1.901	12,7,8
109.022	2.160	12,7,5
110.444	2.189	21,15,24
113.471	2.249	12,7,8
118.231	2.343	12,7,5
119.642	2.371	12,7,5

CONTINUATION STEP NUMBER 41

Value of Lambda is 0.274
Present Continuation Parameter is 14 ;Angle at Bus 15
Next Continuation Parameter Will Be 14 ;Angle at Bus 15
Stepsize is 0.0200

BUS	VOLTAGE	TANGENT COMPONENT	ANGLE	TANGENT COMPONENT	REAL LOAD	REACTIVE LOAD	QC ADDED	GENERATION REAL	GENERATION REACTIVE	REACTIVE INJECTION QC	REACTIVE INJECTION QL
1	1.030	na	-10.99	na	0.000	0.000	0.000	11.282	0.853	0.000	0.000
2	1.024	-0.098	-26.48	0.111	0.000	0.000	0.000	5.299	1.800	0.000	0.000
3	0.981	-0.116	-36.33	-0.173	7.634	0.057	0.000	0.000	0.000	0.000	0.000
4	0.953	-0.140	-37.92	-0.182	11.854	1.991	0.000	0.000	0.000	0.000	0.000
5	0.964	-0.143	-33.06	-0.144	0.000	-0.146	-0.146	0.000	0.000	-0.125	0.000
6	0.971	-0.143	-31.45	-0.133	0.218	0.109	0.000	12.158	3.000	0.000	0.000
7	0.952	-0.145	-35.44	-0.159	5.543	1.086	-0.905	0.000	0.000	-0.138	0.000
8	0.950	-0.143	-35.88	-0.161	12.376	1.042	-0.760	0.000	0.000	0.000	0.000
9	0.989	-0.073	-20.68	-0.047	0.000	0.000	0.000	0.000	0.000	0.000	0.000
10	0.988	-0.140	-27.40	-0.107	0.000	0.000	0.000	13.777	3.000	0.000	0.000
11	0.980	-0.142	-28.80	-0.116	0.000	0.000	0.000	0.000	0.000	0.000	0.000
12	0.960	-0.152	-29.33	-0.121	0.202	1.080	-1.006	0.000	0.000	-0.121	0.000
13	0.978	-0.141	-29.43	-0.122	0.000	0.000	0.000	0.000	0.000	0.000	0.000
14	0.965	-0.137	-34.35	-0.159	0.000	0.000	0.000	0.000	0.000	0.000	0.000
15	0.965	-0.111	-39.11	-0.197	7.587	2.448	-1.179	0.000	0.000	0.000	0.000
16	0.995	-0.090	-36.98	-0.189	7.809	0.766	0.000	0.000	0.000	0.000	0.000
17	0.986	-0.096	-37.76	-0.189	0.000	0.000	0.000	0.000	0.000	0.000	0.000
18	0.979	-0.105	-38.33	-0.189	3.746	0.711	0.000	0.000	0.000	0.000	0.000
19	1.049	-0.097	-28.74	-0.149	0.000	0.000	0.000	13.334	3.000	0.000	0.000
20	0.984	-0.098	-33.13	-0.174	16.121	2.442	0.000	10.714	2.500	0.000	0.000
21	0.998	-0.065	-32.37	-0.172	6.496	1.959	0.768	0.000	0.000	0.000	0.000
22	1.048	-0.027	-22.89	0.143	0.000	0.000	0.000	13.777	4.000	0.000	0.000
23	1.046	na	-23.50	-0.148	5.858	2.006	0.000	11.840	2.927	0.000	0.000
24	1.012	-0.076	-37.10	-0.190	7.316	-3.037	-0.851	0.000	0.000	0.000	0.000
25	1.047	-0.093	-25.93	-0.114	5.311	1.119	0.000	11.410	3.000	0.000	0.000
26	1.007	-0.074	-32.76	-0.162	3.295	0.401	0.000	0.000	0.000	0.000	0.000
27	0.978	-0.090	-38.09	-0.189	6.662	1.790	0.000	0.000	0.000	0.000	0.000
28	1.029	-0.021	-26.80	-0.147	4.884	0.654	0.000	0.000	0.000	0.000	0.000
29	1.051	na	-21.07	-0.136	6.721	0.638	0.000	17.482	1.911	0.000	0.000
30	1.034	-0.043	-16.85	-0.017	0.000	0.000	0.000	0.000	0.000	0.000	0.000

VOLTAGE STABILITY INDEX = 0.0558

WEAKEST LOAD BUSES - ACCORDING TO TANGENT ELEMENTS CORRESPONDING TO VOLTAGE
12 7 5
WEAKEST BUSES - ACCORDING TO TANGENT ELEMENTS CORRESPONDING TO ANGLE
15 24 18

TOTAL REACTIVE CAPACITIVE SUPPLY = -5.616
TOTAL REACTIVE INDUCTIVE SUPPLY = 0.000
NET REACTIVE SUPPLY = -5.616
TOTAL SYSTEM LOAD = 119.642

Figure 5.4 A typical PCOS output table for 30-bus system example

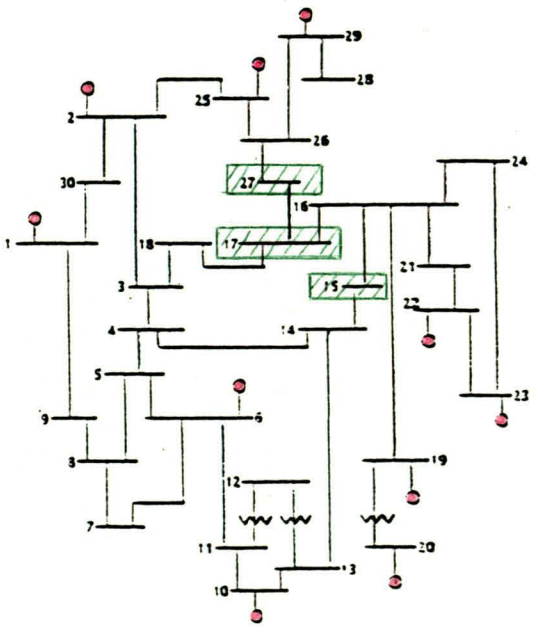

a) base real load

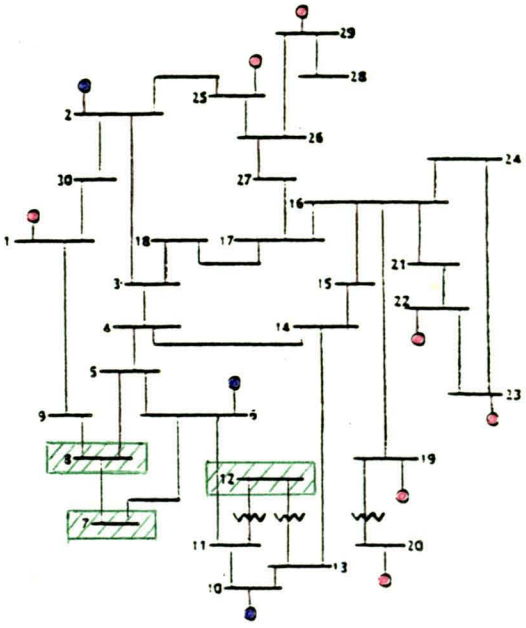

b) 1.901 × base real load

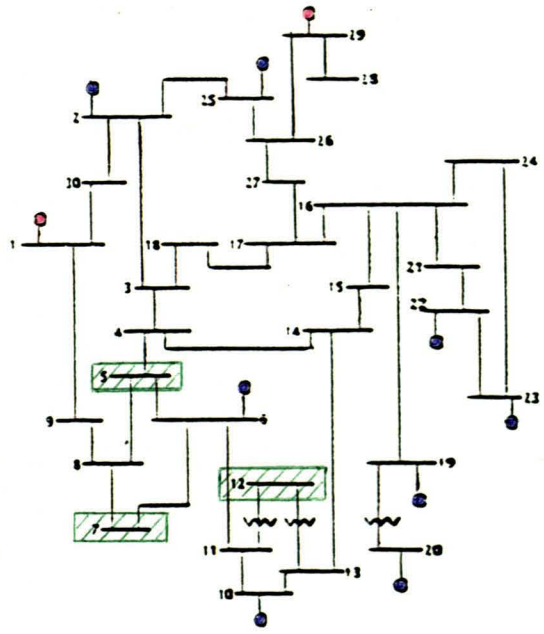

c) 2.371 × base real load

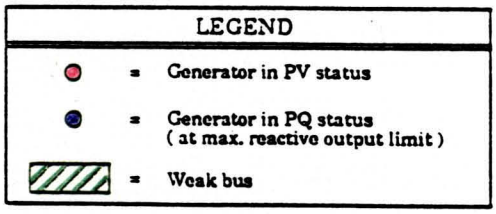

Figure 5.5: Location of the top three weak buses as system load increases

5.4 Implementation of the Relaxation Scheme

Although our goal to maximize real power transfer with minimum amount of shunt reactive power has been achieved, it is essential to realize that the financial loss because of voltage collapse outweighs the savings or earnings through maximum power transfer. One way to prevent voltage collapse is to provide some form of measure or index to predict the coming of voltage collapse.

In chapter 3, the value obtained from $| dP_{TOTAL} / dV_k |$, where k is the weakest bus in the system at each load level, is suggested as a possible voltage stability index. On the other hand, the value of the tangent component $d\lambda$ should also approach zero as the system approaches the critical point. From a computational point of view, the latter approach is more convenient, since $d\lambda$ can be obtained easily after solving for the tangent vector at each load level.

In the last section, a voltage stability index based upon a normalized $d\lambda$ is presented along with an increase of load level for each of the four test systems. Despite its good performance in the PCS, the index derived from the normalized $d\lambda$ fails to provide a good indication for approaching voltage collapse in the PCOS. Also, the index is very sensitive to change in generator status especially when a generator in PQ mode changes to PV mode in the course of computation. Otherwise, the index shows minor deviation in value despite system load continues to increase.

One possible explanation would be the continual improvement of the voltage profile to meet specified voltage limit constraints in optimization. These

voltage corrections may indirectly generate flat tangent vector profiles in the state variables space from which the index is derived.

In view of this, a relaxation scheme (RS) is devised. This scheme, which combines the PCS and PCOS through alternate executions, has two objectives:

- To provide an acceptable index through the execution of the PCS
- To retain the capability of maximizing the real power transfer with minimum amount of reactive support.

This scheme is illustrated in Figure 5.6 and the corresponding flow chart is outlined in Figure 5.7. After testing the RS using the given test systems, the

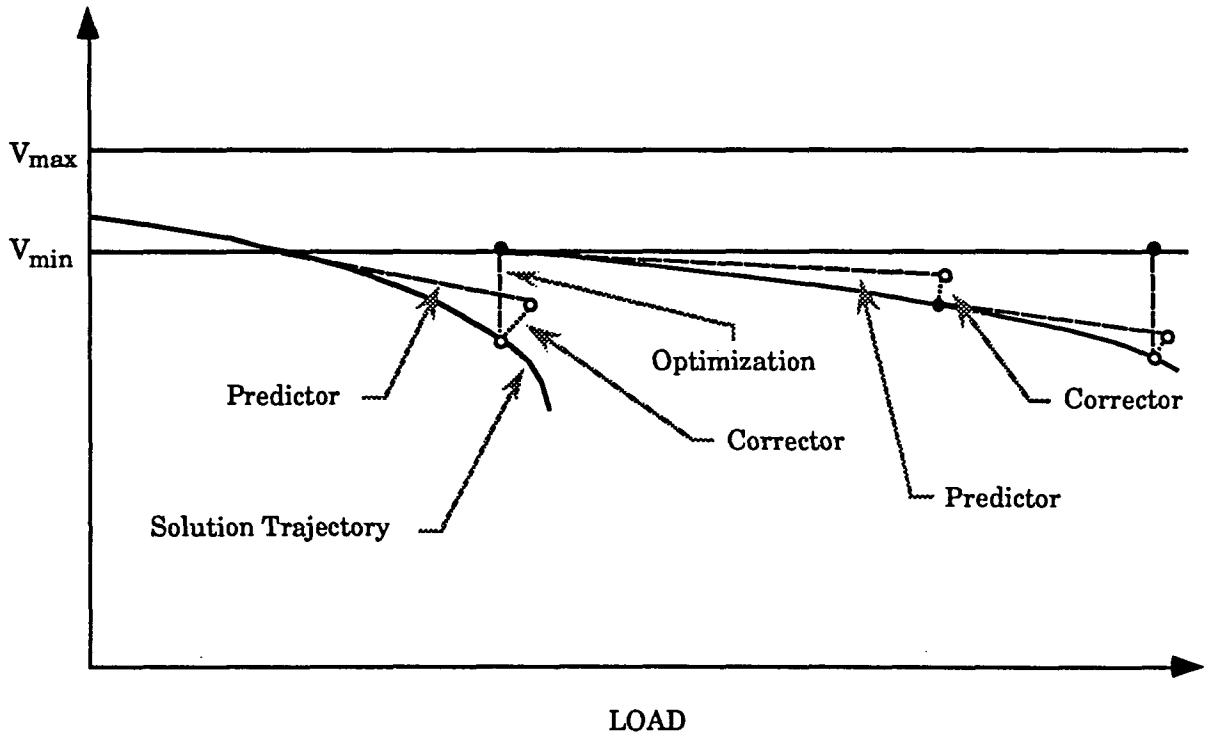

Figure 5.6: An illustration of the relaxation scheme

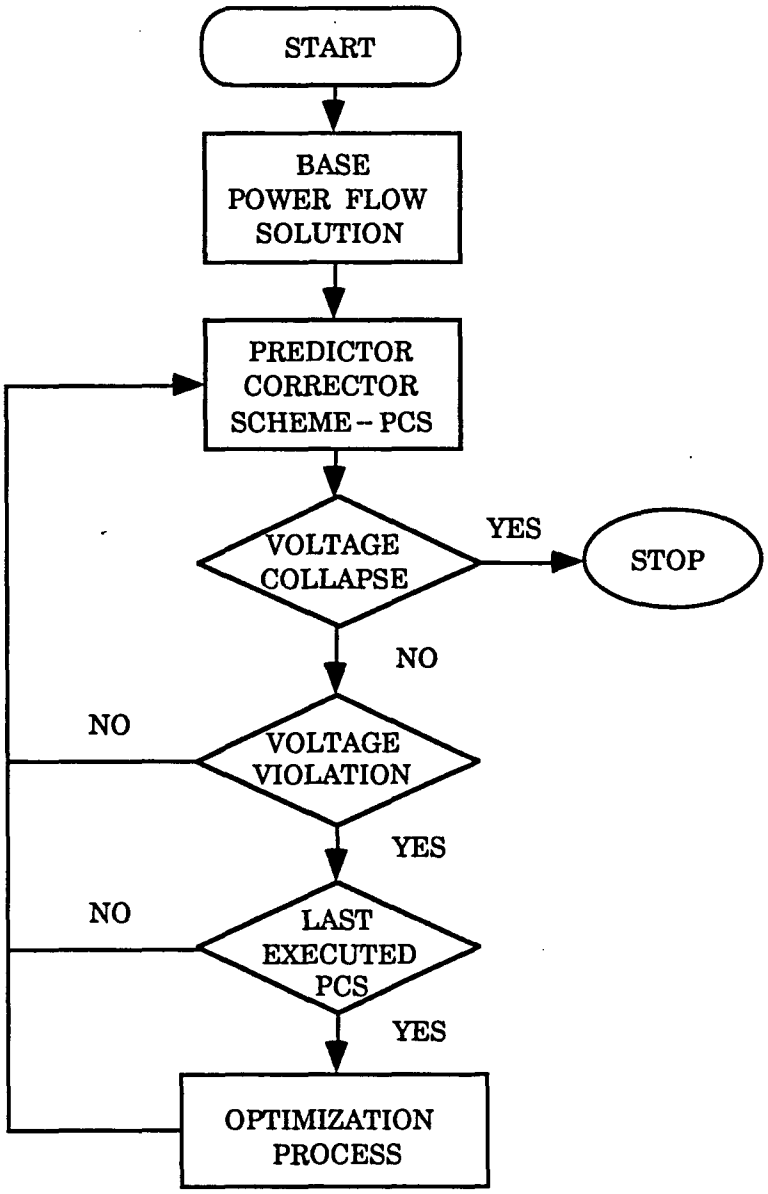

Figure 5.7: Flow chart of the relaxation scheme

Table 5.15: Comparison of the PCS, PCOS, RS using the 2-bus system

METHOD	MAXIMUM SYSTEM REAL POWER TRANSFER IN P.U.*	REACTIVE INJ. IN P.U. CAP. / IND.	WEAK LOAD BUS † LOCATIONS BEFORE VOLTAGE COLLAPSE	LOWEST BUS VOLT. IN P.U.
PCS	0.640	0.000 / 0.000	2	0.814
PCOS	0.794	-0.183 / 0.000	2	0.950
RS	0.780	-0.165 / 0.000	2	0.950

* INITIAL SYSTEM REAL POWER = 0.1 p.u.
† NUMBER OF WEAK LOAD BUSES FOR REACTIVE INJECTION = 1

results are tabulated with that of the PCS and PCOS in Tables 5.15 – 5.18. It can be concluded that the results under RS are generally more conservative than that of the PCOS. Because RS provides a real power transfer level at which a sudden drop of reactive power support will lead to voltage collapse, the value of real power transfer is expected to be smaller.

Table 5.16: Comparison of the PCS, PCOS, RS using the 14-bus system

METHOD	MAXIMUM SYSTEM REAL POWER TRANSFER IN P.U.*	REACTIVE INJ. IN P.U. CAP. / IND.	WEAK BUS † LOCATIONS BEFORE VOLTAGE COLLAPSE	LOWEST BUS VOLT. IN P.U.
PCS	4.382	0.000 / 0.000	14,13,10,12,9	0.594
PCOS	9.444	-8.767 / 0.987	3,4,14,7,9	0.950
RS	9.267	-7.696 / 0.198	3,4,7,14,9	0.950

* INITIAL SYSTEM REAL POWER = 2.590 p.u.
† NUMBER OF WEAK BUSES FOR REACTIVE INJECTION = 5

Table 5.17: Comparison of the PCS, PCOS, RS using the 16-bus system

METHOD	MAXIMUM SYSTEM REAL POWER TRANSFER IN P.U.*	REACTIVE INJ. IN P.U. CAP. / IND.	WEAK LOAD BUS † LOCATIONS BEFORE VOLTAGE COLLAPSE	LOWEST BUS VOLT. IN P.U.
PCS	5.241	-0.000 / 0.000	16,15,2,4,6	0.635
PCOS	9.289	-4.529 / 0.000	16,15,4,2,6	0.950
RS	9.129	-4.272 / 0.000	16,8,14,7,10	0.950

* INITIAL SYSTEM REAL POWER = 4.250 p.u.
† NUMBER OF WEAK LOAD BUSES FOR REACTIVE INJECTION = 5

However, the degree of reduction depends upon the characteristics and the initial state of the system. Using the 30-bus system results in Table 5.18, the maximum real power transfer under PCS and RS are found to be 106.855 and 108.868 p.u. respectively. Though the net increase is only 2.013 p.u., it is a well-known fact that the New England 30-bus system is an initially stressed system.

Table 5.18: Comparison of the PCS, PCOS, RS using the 30-bus system

METHOD	MAXIMUM SYSTEM REAL POWER TRANSFER IN P.U.*	REACTIVE INJ. IN P.U. CAP. / IND.	WEAK LOAD BUS † LOCATIONS BEFORE VOLTAGE COLLAPSE	LOWEST BUS VOLT. IN P.U.
PCS	106.855	0.000 / 0.000	12,7,8,5,11	0.914
PCOS	118.255	-4.990 / 0.000	12,7,8,5,11	0.950
RS	108.868	-1.185 / 0.000	12,7,5,8,11	0.950

* INITIAL SYSTEM REAL POWER = 50.465 p.u.
† NUMBER OF WEAK LOAD BUSES FOR REACTIVE INJECTION = 5

This means the system is more likely to experience voltage collapse if there is a deficiency of reactive power support. Consequently, the MW improvement should not be large as verified by the results in Table 5.18.

Meanwhile, Tables 5.19 – 5.22 demonstrate the significant improvement to the performance of the voltage stability index under the proposed RS. As observed, the performance of the resulting index is comparable with that of the PCS in Tables 5.5, 7, 9, 11 where the indices decrease monotonically with load increases. For example, the voltage stability index for the 30-bus system in Table 5.22 decreases smoothly from 0.1300 to 0.0665 without interruption. However, the sudden change in indices from 0.0665 to -0.0061 deserves further explanation which will be discussed in the assessment section.

Table 5.19: Voltage stability index under RS in the 2-bus system

REAL POWER TRANSFER IN P.U. BEFORE SUDDEN VOLTAGE COLLAPSE	VOLTAGE STABILITY INDEX
0.7059	0.4243
0.7287	0.3452
0.7406	0.2998
0.7547	0.2429
0.7619	0.2121
0.7704	0.1750
0.7748	0.1554
0.7799	0.1323
0.7813	-0.0053

Table 5.20: Voltage stability index under RS in the 14-bus system

REAL POWER TRANSFER IN P.U. BEFORE SUDDEN VOLTAGE COLLAPSE	VOLTAGE STABILITY INDEX
8.4529	0.0736
8.5366	0.0691
8.6500	0.0628
8.7504	0.0572
8.8667	0.0508
8.9656	0.0453
9.0686	0.0395
9.1675	0.0340
9.2667	0.0284
9.2769	-0.0001

Table 5.21: Voltage stability index under RS in the 16-bus system

REAL POWER TRANSFER IN P.U. BEFORE SUDDEN VOLTAGE COLLAPSE	VOLTAGE STABILITY INDEX
8.5417	0.0774
8.6668	0.0672
8.7708	0.0598
8.8582	0.0536
8.9317	0.0484
8.9938	0.0440
9.0464	0.0398
9.0912	0.0367
9.1292	0.0335
9.1405	-0.0004

Table 5.22: Voltage stability index under RS in the 30-bus system

REAL POWER TRANSFER IN P.U. BEFORE SUDDEN VOLTAGE COLLAPSE	VOLTAGE STABILITY INDEX
63.0812	0.1300
68.8484	0.1285
74.5445	0.1269
80.1396	0.1230
85.5849	0.1203
90.9081	0.1174
100.5802	0.0957
104.9210	0.0918
108.8679	0.0665
110.3960	-0.0061

5.5 Assessments

The following assessments are made to capture the experiences gained from the 14-bus system and the various problems encountered in this research.

The AEP 14-bus system has a topology that the loads are concentrated in the northern part of the system; whereas, the generators and synchronous compensators are located to the east and to the south away from the load. Unlike the other systems studied, convergent problem occurs when reactive injection sites are limited to weak load buses only.

Upon examining the problem, it is discovered that the bus voltages at the loads are high at the upper voltage limit and the bus voltages at the synchronous condensers to the south are low at the lower voltage limit. This creates a voltage unbalanced phenomenon across the system. A network constrained problem where further load increase through reactive injection is impossible without violating voltage constraints. By including other weak buses for reactive injection, no convergent problem is reported and a maximum real power transfer has been reached.

Although no network constrained problem is encountered in the 16-bus and 30-bus systems, the results from the 30-bus system reveal that weak buses migrate across the system as load increases. More intriguing, the weakest buses tend to cluster around the generator that has recently reached its maximum reactive limit.

Using the 30-bus system, the effect of increasing the specified number of injection buses to the real power transfer capability is studied. It is found that the real power transfer decreases as the number of injection buses increases. This can be explained by the improvement of the voltage profile because of the larger number of injection sites over a wider system area. With less voltage violations, the amount of reactive power injection decreases accordingly, which indirectly reduces the real power transfer capability of the system.

Another challenge to this research is the poor performance of the voltage stability index following the implementation of the PCOS. Despite continuous load increases, the deviations between each index value is relatively small. Furthermore, the index is very sensitive to changes in generator's status; in which case, the index may suddenly increase or decrease in value without any

trend or pattern whatsoever. As a result, the index becomes very deceitful and fails to provide a good measure to the proximity of voltage collapse.

In view of this, a RS (relaxation scheme) was implemented and tested. Significant improvements have been made and the results are recorded. Unfortunately, the improved index fails to detect a sudden voltage collapse when the system is highly compensated. An index that seemingly implies the current operating point is far away from voltage collapse can suddenly turn negative at the next increment of load. Here, a zero index corresponds the critical point has been reached while a negative index implies the critical point has been passed.

Therefore, in a highly compensated environment, any index that relies on gradient information as a means to measure the proximity to voltage collapse would be deemed as inappropriate and misleading. However, under highly compensated environment, the switch to the direct method and the automatic reduction in step sizes between continuation processes can be implemented as a way to locate the critical point. In closing, the next chapter concludes the entire research effort with highlight on related topics for future studies.

6 CONCLUSIONS AND FUTURE WORK

To prevent voltage collapse from occurring, system operators and planners are looking for analytical tools that can enhance their understanding of where the system is actually operating with respect to the point of collapse – critical point. In addition to knowing the load level where the system will experience voltage collapse, it is of particular interest to determine how much reactive power supply is required and where it should be located so that the power system can be operated at maximum reliability and economy.

A CPF (continuation power flow) was first developed to overcome the ill-conditioning near the critical point; where the Jacobian matrix of the Newton-Raphson method becomes singular. By applying a locally parameterized continuation technique, the CPF initially starts with a known power flow solution and then enters a PCS (predictor-corrector scheme) to find subsequent path-dependent solutions above and below the critical point for a given load increase scenario.

Interfacing with the PCS, this research attempts to develop a methodology that meets the system planners' needs. It first recognizes the sensitivity information derived from CPF as a reliable source for identifying weak buses that are prone to voltage collapse. Then, buses within this set of weak buses are further selected to provide remedial action against voltage collapse. In this research, the idea of shunt reactive power injection at selected weak load buses is proposed and the shunt reactive power resources are treated as infinite.

To achieve an economical solution at a given load level, the proposed method is formulated as an nonlinear constrained optimization problem with an objective that minimizes the amount of shunt reactive power injection. This approach is called the PCOS (predictor-corrector optimization scheme). Not only is the voltage collapse process delayed by the injection of reactive power, but the active power transfer capability of the system is improved also. Furthermore, bus voltages are ensured within permissible voltage operating limits. This makes the proposed strategy specially attractive for those utilities interested in economic transfer but hindered by the steady-state voltage instability problem. Chapter 5 illustrates the proposed PCOS with tabulated results.

Unfortunately, the voltage stability index derived from the CPF fails to provide a good measure to voltage collapse. One possible explanation would be the continual improvement of the voltage profile to meet specified voltage limit constraints in optimization. These voltage corrections may indirectly generate flat tangent vector profiles in the state variable space from which the index is derived. As a result, a RS (relaxation scheme) is suggested to improve the performance of the voltage stability index. With the RS, the performance of the voltage stability index does improve significantly. Like any index that relies on sensitivity or gradient information, the voltage stability index is incapable of foretelling sudden collapse as discovered in the results. To tackle this, reduction in step sizes and switching to the direct method are suggested to locate the critical point.

Nevertheless, the maximum load level obtained from RS actually represents the load level beyond which a sudden drop of reactive support in the system may lead to sudden voltage collapse. Since no system operates in perfect

condition, this indirectly provides a built-in security margin to forewarn possible sudden voltage collapse.

Finally, it is important to realize that every system is unique and it is possible to encounter network constrained problem before maximum load level can be reached. This further implies that a good knowledge of the system topology and behavior at various operating conditions is essential to the operation of maximum reliability and economy. In terms of contributions, this research:

- Extends the capability of the continuation power flow to the capacitor placement problem
- Explores the possibility of achieving maximum real power transfer while minimizing the amount of shunt reactive support to a given system
- Preserves the performance of a voltage stability index using a relaxation scheme
- Establishes a built-in security margin to guard against sudden voltage collapse
- Illustrates the fact that under highly capacitive compensated environment, gradient based stability index is incapable of detecting sudden voltage collapse
- Provides an important insight into the optimal capacitor placement problem through the encounter of network constrained problem

At this point, the work of this research has been documented. However, more work is necessary to carry the ideas developed in this research into a realistic environment. Consequently, the following topics are of major interest:

- Modelling of the static VAr compensator (SVC) taking consideration of the voltage dependent characteristics
- Incorporation of the actual capacitor bank limits
- Integration of the continuation and optimization techniques with the aim of attaining a continuous optimal solution path

BIBLIOGRAPHY

[1] Taylor, C. W. *Reactive Power Compensation and Voltage Stability: Removing Transmission Limitations*. Portland: Carson Taylor Seminar, June 1989.

[2] VanCustem, T. "A Method to Compute Reactive Power Margins With Respect to Voltage Collapse," paper no. 90 WM 097-6-PWS, *IEEE Winter Meeting*, Atlanta, Ga., Feb. 1990.

[3] Obadina, O. O. and G. J. Berg. "Determination of Voltage Stability Limit in Multimachine Power Systems," *IEEE Trans. on PWRS*, Vol. 3, No. 4 (Nov. 1988): 1545-1554.

[4] Ajjarapu, V. "Identification of Steady-State Volage Stability in Power Systems," *International Journal of Energy Systems*, Vol. 11, No. 1 (1991): 43-46.

[5] Alvarado, F., and T. Jung. "Direct Detection of Voltage Collapse Conditions." *Proceedings: Bulk Power System Voltage Phenomena – Voltage Stability and Security. EPRI Report EL - 6183*, Sept. 19-24, 1988, 5-23 – 5-38. Fairfax: Carlsen & Fink Associates, 1989.

[6] Obadina, O. O., and G. J. Berg. "VAR Planning for Power System Security," *IEEE Trans. on PWRS*, Vol. 4, No. 2 (May 1989): 677-686.

[7] Semlyen, A., B. Gao, and W. Janischewskyi. "Calculation of the Extreme Loading Condition of a Power System for the Assessment of Voltage Stability," *IEEE Trans. on PWRS*, Vol. 6, No. 2 (Feb. 1991): 307-315.

[8] Iba, K., H. Suzuki, M. Egawa, and T. Watanabe. "Calculation of Critical Loading Condition With Nose Curse Using Homotopy Continuation Method," *IEEE Trans. on PWRS*, Vol. 6, No. 2 (May 1991): 584-593.

[9] Ajjarapu, V., and C. Christy. "The Continuation Power Flow – A Tool for Steady State Voltage Stability Analysis." *Proceedings of 1991 PICA Conference*. May 7-10, 1991, pp. 304-311. New York: IEEE, 1991.

[10] Reason, J. "Voltage Security: The Hidden Threat to Transmission Networks," *Electrical World* 203 (April 1989): 51-53.

[11] Miller, T. J. *Reactive Power Control in Electric Systems*. New York: John Wiley & Sons Inc., 1982.

[12] *Proposed Terms and Definitions for Power System Stability*, by the Task Force on Terms and Definitions, System Dynamic Performance Subcommittee PES, *IEEE Trans. on PAS*,Vol. PAS-101 (1982): 1894-1898.

[13] Mansour, Y., ed. "Voltage Stability of Power Systems: Concepts, Analytical Tools and Industry Experience," System Dynamic Performance Subcommittee, Power System Engineering Committee, PES, IEEE, New York, NY, 1991.

[14] Kimbark, E. W. *Power System Stability Vol. I Elements of Stability Calculations*. New York: John Wiley & Sons Inc., 1948.

[15] Kimbark, E. W. *Power System Stability Vol. III Synchronous Machine*. New York: John Wiley & Sons Inc., 1956.

[16] Ajjarapu, V., and B. Lee. "Bifurcation Theory and its Application to Nonlinear Dynamical Phenomena in an Electrical Power System." *Proceedings of 1991 PICA Conference*. May 7-10, 1991, pp. 312-31. New York: IEEE, 1991.

[17] Garcia, C. B., and W. I. Zangwill. *Pathways to Solutions, Fixed Points and Equilibria*. Englewood Cliffs, NJ: Prentice-Hall Inc., 1981.

[18] Fahmideh-Vojdani A., and F. D. Galiana. "The Continuation Method and its Application to System Planning and Operation," Paper 102-04, *Proceedings of the CIGRE*, Florence, Italy, 1983.

[19] Huneault, M., A. Fahmideh-Vojdani, M. Juman, R. Calderon and F. D. Galiana. "The Continuation Method in Power System Optimization: Applications to Economy-Security Functions," *IEEE Trans. on PAS*, Vol. PAS-104 (Jan. 1985): 114-124.

[20] Huneault, M., and F.D. Galiana. "An Investigation of the solution to the Optimal Power Flow Problem Incorporating Continuation Method," paper no. 89 SM 694-1-PWRS, *IEEE Summer Meeting*, Long Beach, CA, June 1989.

[21] Christy, C. D. "Analysis of Steady State Voltage Stability in Large Scale Power Systems." M.S. Thesis, Iowa State University, Ames, IA, 1990.

[22] Seydel, R. *From Equilibrium to Chaos*, New York: Elsevier, 1988.

[23] Carpentier, J. "Optimal Power Flows," *Electrical Power and Energy System*, No.1 (April 1979): 3-15.

[24] Dommel, H.W., and W. F. Tinney. "Optimal Power Flow Solutions," *IEEE Trans. on PAS*, Vol. PAS-87 (Oct 1968): 1866-1876.

[25] IEEE, Baltimore Chapter, *Tutorial on Advanced Optimization Techniques*, 1991 PICA Conference, Power Technologies, Inc., Schenectady, NY.

[26] Huneault, M., and F.D. Galiana. "A Survey of the Optimal Power Flow Literature," *IEEE Trans. on PWRS*, Vol. 6, No.2 (May, 1991): 762-770.

[27] Scott, B., J.L. Marinho. "Linear Programming for Power System Network Security Application," *IEEE Trans. on PAS* Vol. PAS-98, No. 3 (May/June, 1979): 837-848.

[28] Kirschin, D.S., H.P. Van Meeteren. "MW/Voltage Control in Linear Programming Based Optimal Power," *IEEE Trans. on PWRS*, Vol.3, No.2 (May, 1988): 579-584.

[29] Snyder, W. L. Jr. "Linear Programming Adapted for Optimal Power Flow," *IEEE Tutorial Publication - Application of Optimization Methods for Economy/Security Functions in Power System Operations*, 90EH0328-5-PWR, IEEE, New York, NY.

[30] Burchett, R.C., H. H. Happ, D.R. Vierath, and K.A. Wirgau. "Developments in Optimal Power Flow," *IEEE Trans. on PAS*, Vol. PAS-101, No.2 (Feb.,1982): 406-414.

[31] Rehn, C. J., J. A. Bubenko, and D. Sjelvgren. "Voltage Optimization Using Augmented Lagrangian Functions and Quasi-Newton Techniques," *IEEE Trans. on PWRS*, Vol. 4, No. 4 (1989): 1470-1483.

[32] Sun, D.I., B. AShley, B. Brewer, A. Hughes, and W.F. Tinney. "Optimal Power Flow Solution by Newton Approach," *IEEE Trans. on PAS* Vol. PAS-103, No. 10 (Oct. 1984): 2864-2880.

[33] Sun, D.I., B. Hughes, W.F. Tinney, J. M. Bright, and J. Lamont. "Optimal Power Flow Solution by Newton's Method," *IEEE Tutorial Publication - Reactive Power: Basics, Problems and Solutions*," 87EH0262-6-PWR, IEEE, New York, NY.

[34] Burchett, R.C., H.H. Happ, and D.R. Vierath. "Quadratically Convergent Optimal Power Flow," *IEEE Trans. on PAS*, Vol. PAS-103, No.11 (Nov. 1984): 3267-3275.

[35] *Fortran Library Manual*, Mark 13, Vol. 4, Numerical Algorithm Group (NAG), 1988.

[36] Stevenson, W. D. *Elements of Power System Analysis, 4th ed.* New York: McGraw Hill Inc., 1982.

[37] Heydt, G. T. *Computer Analysis Methods For Power System*. New York: Macmillian Publishing Co., 1986.

[38] Anderson, P. M. *Analysis of Faulted Power System*. Ames: The Iowa State University Press, 1973.

[39] Gross, C. A. *Power System Analysis, 2nd ed.* New York: John Wiley & Sons Inc., 1986.

[40] Stagg, G. W., and A. H. El-Abiad. *Computer Methods in Power System Analysis.* New York: McGraw Hill Inc., 1968.

[41] Kusic, G. L. *Computer-Aided Power System Analysis*. Englewood Cliff, NJ: Prentice-Hall Inc., 1986.

[42] Debs, A. S. *Modern Power System Control and Operations*,. Boston: Kluwer Academic Publisher, 1988.

[43] Wood, A. J., and B. F. Wollenberg. *Power Generation Operation and Control*. New York: John Wiley and Sons Inc., 1984.

[44] Pierson, B.L. "Sequential Quadratic Programming and its use in Optimal Control Model Comparisons," *Optimal Control Theory and Economic Analysis 3*. Elsevier Science Publishers B.V. (North-Holland), (1988): 175-193.

[45] Gill, P.E., W. Murray, and M.H. Wright. *Practical Optimization*. Academic Press, New York, 1981.

[46] Luenberger, D. G. *Linear and Nonlinear Programming*, 2ed. Addison-Wesley Publishing Co., Massachusetts, 1984.

[47] Fletcher, R. *Practical Methods of Optimization*. John Wiley & Sons Inc., New York, 1987.

[48] Wallach, Y. *Calculations and Programs for Power System Networks*, Englewood Cliffs N.J.: Prentice-Hall Inc., 1986.

[49] Schlueter, R. A., A.G. Costi, J.E. Sekerke, and H.L. Forey.*Voltage Stability and Security Assessment*, EPRI Publication EL-5967, August, 1988.

ACKNOWLEDGMENTS

It is my pleasure to have Dr. V. Ajjarapu as my major professor whose constant attention and advice to this research are immeasureable. Through the many hours of research and discussion, I have learned how to approach and think about a particular problem from various perspectives. His dedication and interest to the study of voltage stability will forever be my learning example.

Next, I would like to thank Dr. John Lamont, director of the Electric Power Research Center (EPRC), for his assistance, encouragement and guidance throughout my graduate studies.

Special thank to Dr. Bion Pierson of the Aerospace Engineering Dept. who out of his busy schedule offers his time to be my Graduate Committee Member.

In addition, I would like to extend my special thank to Dr. Ken Krumpel who has been very instrumental in giving insight and assistance to the problems I encountered in learning power systems ever since I was an undergraduate student at Iowa State University.

Finally, I am indebted to the Power Affliate Program at Iowa State University for the financial support during my graduate studies.

APPENDIX A

CALCULATION OF THE SINGULAR JACOBIAN MATRIX USING THE 2-BUS SYSTEM WITH INFINITE SOURCE

As a part of the formulation of the Newton-Raphson power flow method given in Appendix B, we will apply this method directly to the 2-bus power flow problem. For the k-th bus, we adopt these notations as

$$V_k = |V_k| \angle \delta k \,,\; V_n = |V_n| \angle \delta n \,,\; Y_{kn} = |Y_{kn}| \angle \theta kn \qquad (A.1)$$

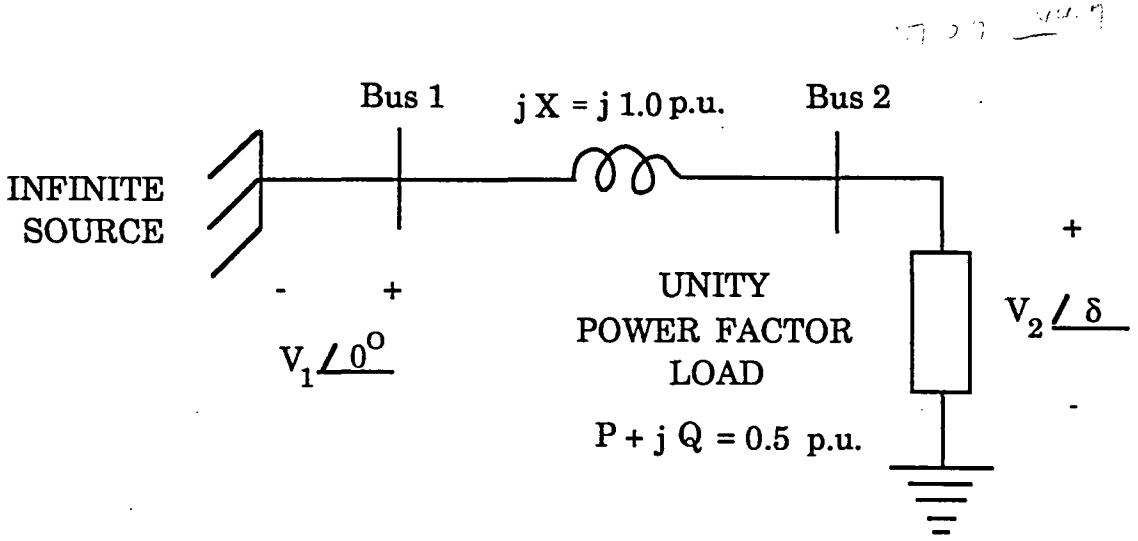

Figure A.1: 2-bus system at maximum unity power power factor load

At the load bus, we have the following power flow equations

$$P_2 = P_{G2} - P_{L2} - P_{T2} = 0 \tag{A.2}$$

$$Q_2 = Q_{G2} - Q_{L2} - Q_{T2} = 0 \tag{A.3}$$

where

$$P_{T2} = \sum_{n=1}^{2} |V_2| \cdot |V_n| \cdot |Y_{2n}| \cdot \cos \angle \delta 2 - \delta n - \theta 2n \tag{A.4}$$

$$Q_{T2} = \sum_{n=1}^{2} |V_2| \cdot |V_n| \cdot |Y_{2n}| \cdot \sin \angle \delta 2 - \delta n - \theta 2n \tag{A.5}$$

Notice that the power flow equations at the slack bus are not considered in the formulation of the Jacobian matrix. However, the effects of the voltage and angle of the slack bus are taken into account when the power flow equations of the other buses are being formed.

For the given 2-bus system with $V_1 = V_2 = 1.0$ p.u., $X = 1.0$ p.u. at maximum unity power factor load of $P = 0.5$ p.u., the corresponding admittance matrix is

$$Y_{bus} = \begin{bmatrix} 1.0\angle -90^0 & 1.0\angle 90^0 \\ 1.0\angle 90^0 & 1.0\angle -90^0 \end{bmatrix} \tag{A.6}$$

$$\frac{\partial P_2}{\partial \delta_2} = |V_2| \cdot |V_1| \cdot |Y_{21}| \cdot \sin(\delta_2 - \delta_1 - \theta_{12}) = \frac{1}{\sqrt{2}} \cdot \sin(-135^0)$$

$$= \frac{-1}{2} \tag{A.7}$$

$$\frac{\partial P_2}{\partial V_2} = -|V_1| \cdot |Y_{21}| \cdot \cos(\delta_2 - \delta_1 - \theta_{12}) - 2 \cdot |V_2| \cdot |Y_{22}| \cdot \cos(-\theta_{22})$$

$$= -1.0 \cdot \cos(-135^0) = \frac{1}{\sqrt{2}} \tag{A.8}$$

$$\frac{\partial Q_2}{\partial \delta_2} = -|V_2| \cdot |V_1| \cdot |Y_{21}| \cdot \cos(\delta_2 - \delta_1 - \theta_{12}) = \frac{-1}{\sqrt{2}} \cdot \sin(-135^0)$$

$$= \frac{1}{2} \tag{A.9}$$

$$\frac{\partial Q_2}{\partial V_2} = -|V_1| \cdot |Y_{21}| \cdot \sin(\delta_2 - \delta_1 - \theta_{12}) - 2 \cdot |V_2| \cdot |Y_{22}| \cdot \sin(-\theta_{22})$$

$$= -1.0 \cdot \sin(-135^0) \cdot \frac{-2}{\sqrt{2}} = \frac{-1}{\sqrt{2}} \tag{A.10}$$

Collecting the above partial derivatives, we have the following Jacobian matrix,

$$J = \begin{bmatrix} \frac{\partial P}{\partial \delta} & \frac{\partial P}{\partial V} \\ \frac{\partial Q}{\partial \delta} & \frac{\partial Q}{\partial V} \end{bmatrix} = \begin{bmatrix} \frac{-1}{2} & \frac{1}{\sqrt{2}} \\ \frac{1}{2} & \frac{-1}{\sqrt{2}} \end{bmatrix} \qquad \text{(A.11)}$$

APPENDIX B

THE NEWTON-RAPHSON POWER FLOW METHOD

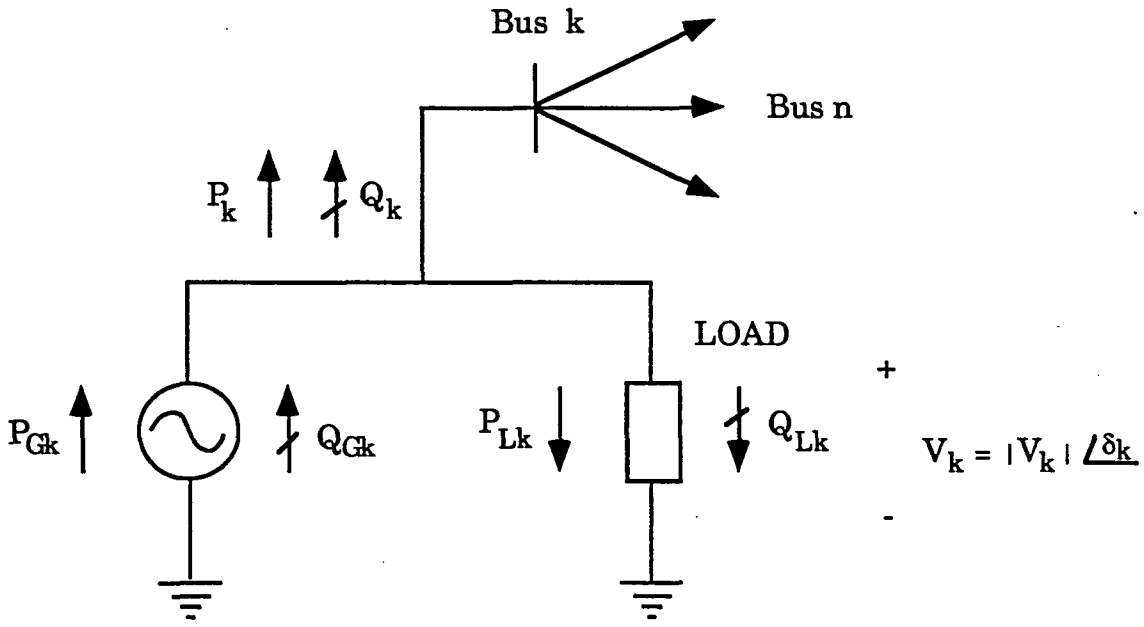

Figure B.1: Variables at a bus

To begin a power flow study, we need to defined the type of buses that are in a given system [36-43]:

1. A load bus (or PQ bus) for which the active and reactive power P and Q are known, and $|V|$ and δ are to be obtained from power flow.

2. A generator bus (or voltage regulated bus) is a bus for which the magnitude of the generated (or specified) voltage $|V|$ and the corresponding generated (or specified) power P are known and Q and δ are to be found. This bus is also called the PV bus.

3. A swing bus (or slack bus) is a generator bus at which $|V|$ and δ are specified, and P and Q are to be calculated. $V\angle\delta = 1\angle 0^{\circ}$ p.u. is often being used as a reference for the power flow calculation. However, it is not compulsory and it is possible to have more than one slack bus in a large system.

When the reactive power limit is reached at a PV bus, the status of this bus should then be switched from PV to PQ since the voltage can no longer be controlled. Similarly, a voltage regulated bus or a generator bus in PQ status can switch its status into PV depending on the flow of the real and reactive power in the system.

Besides knowing the status of each bus, we need to establish the bus admittance (or the Y_{bus}) matrix of a given network. The Y_{bus} matrix can be constructed from the line and transformed input data. The elements of Y_{bus} matrix are formulated using the following guidelines:

Diagonal element: Y_{kk} = sum of admittance connected to bus k

Off-diagonal element: Y_{kn} = – (sum of admittance connected between bus k and bus n) for $k \neq n$.

In many situation, solving nonlinear algebraic equation of the form:

$$\mathbf{F}(\mathbf{x}) = \mathbf{0} \tag{B.1}$$

requires iterative technique where $\mathbf{F}$ denotes the set of nonlinear equation and $\mathbf{x}$ represents the vector of unknowns to be found. Considering the Taylor's series expansion about a value $\mathbf{x}^k$ where k is the current iteration:

$$\mathbf{F}(\mathbf{x}) = \mathbf{F}(\mathbf{x}^k) + \nabla\mathbf{F}(\mathbf{x}^k)\cdot(\mathbf{x} - \mathbf{x}^k) + (1/2)\cdot\nabla^2\mathbf{F}(\mathbf{x}^k)\cdot(\mathbf{x} - \mathbf{x}^k)^2 + \ldots \tag{B.2}$$

If the higher order terms are neglected and further assume that $\mathbf{x}^k$ is close to $\mathbf{x}$ then the nonlinear algebraic equations can be approximated by

$$\mathbf{F}(\mathbf{x}) = \mathbf{F}(\mathbf{x}^k) + \nabla\mathbf{F}(\mathbf{x}^k)\cdot(\mathbf{x} - \mathbf{x}^k) = \mathbf{0} \tag{B.3}$$

$$\mathbf{x} = \mathbf{x}^k - \nabla\mathbf{F}(\mathbf{x}^k)^{-1}.\mathbf{F}(\mathbf{x}^k) \tag{B.4}$$

where the gradient matrix, $\nabla\mathbf{F}(\mathbf{x}^k)^{-1}$, is also referred as the Jacobian matrix, $J(\mathbf{x}^k)$.

To achieve an acceptable accuracy, one must perform iterative calculation on Equation (B.4) and rewrite it as

$$\mathbf{x} = \mathbf{x}^k - \Delta\mathbf{x}^k \tag{B.5}$$

until

(1) $\Delta\mathbf{x}^k$ is smaller than a specified lower bound tolerance

(2) $\Delta\mathbf{x}^k$ is larger than a specified upper bound tolerance

(3) k is greater than a specified maximum iteration

In power system, the real(active) and reactive power flow at any node is assumed to be balanced at all time.

$$P_{Gi} - P_{Li} - P_{Ti} = 0 = \Delta P_i \tag{B.6}$$

$$Q_{Gi} - Q_{Li} - Q_{Ti} = 0 = \Delta Q_i \tag{B.7}$$

where G, L, T denote generation, load demand and transmission respectively. The complex transmitted power, S_{Ti}:

$$S_{Ti} = P_{Ti} + j\,Q_{Ti} = V_i \cdot I_{Ti}^* \tag{B.8}$$

$$I_{Ti} = \sum_{j=1}^{n} Y_{ij} \cdot V_j \qquad i = 1, \ldots, n \tag{B.9}$$

$$I_{Ti}^* = \sum_{j=1}^{n} |Y_{ij}| \cdot |V_j| \, \underline{/-\gamma_{ij} - \delta_j} \tag{B.10}$$

$$S_{Ti} = \sum_{j=1}^{n} |V_i| \cdot |V_j| \cdot |Y_{ij}| \, \underline{/\delta_i - \delta_j - \gamma_{ij}} \tag{B.11}$$

By separating S_{Ti} into P_{Ti}, Q_{Ti}, we have

$$P_{Ti} = \sum_{j=1}^{n} |V_i| \cdot |V_j| \cdot |Y_{ij}| \cos(\delta_i - \delta_j - \gamma_{ij}) \tag{B.12}$$

$$Q_{Ti} = \sum_{j=1}^{n} |V_i| \cdot |V_j| \cdot |Y_{ij}| \sin(\delta_i - \delta_j - \gamma_{ij}) \tag{B.13}$$

To implement the Newton-Raphson method to solve the power flow equations, we define the following:

$$\mathbf{F}(\mathbf{x}) = \begin{Bmatrix} P_{Gi} - P_{Li} - P_{Ti} \\ Q_{Gi} - Q_{Li} - Q_{Ti} \end{Bmatrix} = \mathbf{0} \tag{B.14}$$

and the recursive calculation becomes

$$\begin{bmatrix} \Delta\delta \\ \Delta V \end{bmatrix} = - \begin{bmatrix} \\ J^k \\ \\ \end{bmatrix}^{-1} \cdot \begin{bmatrix} \Delta P^k \\ \Delta Q^k \end{bmatrix} \tag{B.15}$$

with the update

$$\delta_i^{k+1} = \delta_i^k + \Delta\delta_i \tag{B.16}$$

$$V_i^{k+1} = V_i^k + \Delta V_i \tag{B.17}$$

where J is the Jacobian and further divided into four quadrants:

$$J = \left[\begin{array}{c:c} J1 & J2 \\ \hdashline J3 & J4 \end{array}\right] = \left[\begin{array}{c:c} \left[\frac{\partial P}{\partial \delta}\right] & \left[\frac{\partial P}{\partial V}\right] \\ \hdashline \left[\frac{\partial Q}{\partial \delta}\right] & \left[\frac{\partial Q}{\partial V}\right] \end{array}\right] \tag{B.18}$$

and the required partial derivatives are

$$J1(i,i) = \partial P_i / \partial \delta_i = \sum_{\substack{j=1 \\ \neq i}}^{n} |V_i| \cdot |V_j| \cdot |Y_{ij}| \cdot \sin(\delta_i - \delta_j - \gamma_{ij}) \qquad \text{(B.19)}$$

$$J1(i,k) = \partial P_i / \partial \delta_k = -|V_i| \cdot |V_k| \cdot |Y_{ik}| \cdot \sin(\delta_i - \delta_k - \gamma_{ik}) \quad (k \neq i) \qquad \text{(B.20)}$$

$$J2(i,i) = \partial P_i / \partial V_i = -\sum_{\substack{j=1 \\ \neq i}}^{n} |V_j| \cdot |Y_{ij}| \cdot \cos(\delta_i - \delta_j - \gamma_{ij}) - 2 \cdot |V_i| \cdot |Y_{ii}| \cdot \cos(-\gamma_{ii}) \qquad \text{(B.21)}$$

$$J2(i,k) = \partial P_i / \partial V_k = -|V_i| \cdot |Y_{ik}| \cdot \cos(\delta_i - \delta_k - \gamma_{ik}) \qquad (k \neq i) \qquad \text{(B.22)}$$

$$J3(i,i) = \partial Q_i / \partial \delta_i = -\sum_{\substack{j=1 \\ \neq i}}^{n} |V_i| \cdot |V_j| \cdot |Y_{ij}| \cdot \cos(\delta_i - \delta_j - \gamma_{ij}) \qquad \text{(B.23)}$$

$$J3(i,k) = \partial Q_i / \partial \delta_k = |V_i| \cdot |V_k| \cdot |Y_{ik}| \cdot \cos(\delta_i - \delta_k - \gamma_{ik}) \quad (k \neq i) \qquad \text{(B.24)}$$

$$J4(i,i) = \partial Q_i / \partial V_i = - \sum_{\substack{j=1 \\ \neq i}}^{n} |V_j| \cdot |Y_{ij}| \cdot \sin(\delta_i - \delta_j - \gamma_{ij})$$

$$- 2 \cdot |V_i| \cdot |Y_{ii}| \cdot \sin(-\gamma_{ii}) \qquad \text{(B.25)}$$

$$J4(i,k) = \partial Q_i / \partial V_k = - |V_i| \cdot |Y_{ik}| \cdot \sin(\delta_i - \delta_k - \gamma_{ik}) \qquad (k \neq i) \qquad \text{(B.26)}$$

The size of the Jacobian depends on the number of PQ buses, n_{PQ} and the number of PV buses, n_{PV} with total number of buses, $n = n_{PQ} + n_{PV} + 1$. The $\Delta\delta$ vector contains n-1 elements with the slack bus excluded. Whereas, the ΔV vector contains only n_{PQ} elements. Therefore, the Jacobian has a dimension of $(2\, n_{PQ} + n_{PV}) \times (2\, n_{PQ} + n_{PV})$.

APPENDIX C

SEQUENTIAL QUADRATIC PROGRAMMING

Consider the nonlinear problem with equality constraints:

$$\min \quad \mathbf{f}(\mathbf{x}) \tag{C.1}$$

subject to

$$\mathbf{h}(\mathbf{x}) = \mathbf{0}$$

To solve the problem posed by Equation (C.1), we intend to solve a sequence of simpler subproblems that quadratically converge to the solution of the original problem. The concept of SQP is revealed by forming the Lagrangian function, **L**

$$\mathbf{L}(\mathbf{x}, \lambda) = \mathbf{f}(\mathbf{x}) - \lambda^T \mathbf{h}(\mathbf{x}) \tag{C.2}$$

In order to satisfy the necessary condition for minimum, we further differentiate **L** with respect to both the variable vector **x** and multiplier vector λ. Let $\nabla \mathbf{f}(\mathbf{x}) = \nabla \mathbf{f}$, $\nabla \mathbf{h}(\mathbf{x}) = \nabla \mathbf{h}$.

$$\nabla_x \mathbf{L} = \nabla \mathbf{f}^T(\mathbf{x}) - \nabla \mathbf{h}^T(\mathbf{x})\lambda = \mathbf{0} \tag{C.3}$$

$$\nabla_\lambda \mathbf{L} = -\mathbf{h} = \mathbf{0} \tag{C.4}$$

or $$\nabla \mathbf{L}(\mathbf{x}^*, \lambda^*) = \mathbf{0} \tag{C.5}$$

One way to solve these equations is to apply Newton's Method to update x, λ. This is achieved using the Taylor first order expansion.

$$[\nabla \mathbf{L}(\mathbf{x}_k + \partial \mathbf{x}_k, \lambda_k + \partial \lambda_k)]^T = \nabla \mathbf{L}_k^T + \nabla^2 \mathbf{L}_k(\partial \mathbf{x}_k, \partial \lambda_k)^T \tag{C.6}$$

and set the left-hand side $\nabla \mathbf{L}_{k+1}^T = \mathbf{0}$. This becomes

$$\mathbf{0} = \nabla \mathbf{L}_k^T + \nabla^2 \mathbf{L}_k(\partial \mathbf{x}_k, \partial \lambda_k)^T \tag{C.7}$$

$$\nabla^2 \mathbf{L}_k \begin{pmatrix} \partial \mathbf{x}_k \\ \partial \lambda_k \end{pmatrix} = -\nabla \mathbf{L}_k^T \tag{C.8}$$

with

$$\nabla^2 \mathbf{L}_k = \begin{pmatrix} \nabla^2 \mathbf{f} - \lambda^T \nabla \mathbf{h} & -\nabla \mathbf{h}^T \\ -\nabla \mathbf{h} & 0 \end{pmatrix} = \begin{pmatrix} \nabla_{\mathbf{x}}^2 \mathbf{L} & \nabla_{\mathbf{x}\lambda}^2 \mathbf{L} \\ \nabla_{\lambda \mathbf{x}}^2 \mathbf{L} & \nabla_\lambda^2 \mathbf{L} \end{pmatrix} \tag{C.9}$$

Similarly, Equation (C.8) can be written as

$$\begin{pmatrix} \nabla^2 f_k - \lambda_k^T \nabla \mathbf{h}_k & -\nabla \mathbf{h}_k^T \\ -\nabla \mathbf{h}_k & 0 \end{pmatrix} \begin{pmatrix} \partial \mathbf{x}_k \\ \partial \lambda_k \end{pmatrix} = - \begin{pmatrix} \nabla f_k^T - \nabla \mathbf{h}_k^T \lambda_k \\ -\mathbf{h}_k \end{pmatrix} \qquad \text{(C.10)}$$

which is the linearized necessary condition. Solving Equation (C.11) iteratively, we obtain the iterants

$$\begin{aligned} \mathbf{x}_{k+1} &= \mathbf{x}_k + \partial \mathbf{x}_k \\ \lambda_{k+1} &= \lambda_k + \partial \lambda_k \end{aligned} \qquad \text{(C.11)}$$

which eventually should approach $\mathbf{x}^*$ and λ^*. This approach is called the Lagrange-Newton method for solving the constrainted problem of Equation (C.1). The solution is unique if $-\nabla \mathbf{h}^*$ has full rank and $\nabla_{\mathbf{x}}^2 \mathbf{L}$ is positive definite (P.D.) on the tangent space. If we rewrite Equation (C.10) explicitly as

$$\begin{aligned} \nabla_{\mathbf{x}}^2 \mathbf{L}\, \partial \mathbf{x}_k + \nabla f_k^T - \nabla \mathbf{h}_k^T (\lambda_k + \partial \lambda_k) &= \mathbf{0} \\ -\nabla \mathbf{h}_k\, \partial \mathbf{x}_k - \mathbf{h}_k &= \mathbf{0} \end{aligned} \qquad \text{(C.12)}$$

and observe that they may be viewed as the Kuhn-Tucker conditions of the quadratic model

$$\min_{\partial \mathbf{x}_k} \left[\nabla f_k \partial \mathbf{x}_k + \frac{1}{2} \partial \mathbf{x}_k^T \mathbf{B}_k \partial \mathbf{x}_k \right] \qquad \text{(C.13)}$$

subject to

$$\nabla \mathbf{h}_k \partial \mathbf{x}_k + \mathbf{h}_k = \mathbf{0} \tag{C.14}$$

then the Lagragian function of the above quadratic model becomes

$$\tilde{\mathbf{L}} = \nabla f_k \partial \mathbf{x}_k + \frac{1}{2} \partial \mathbf{x}_k^T \mathbf{B}_k \partial \mathbf{x}_k - \mu \left[\nabla_k \mathbf{h} \ \partial \mathbf{x}_k + \mathbf{h}_k \right] \tag{C.15}$$

and the necessary condition are

$$\nabla_{\partial \mathbf{x}} \tilde{\mathbf{L}}^T = \nabla f_k^T + \mathbf{B}_k \partial \mathbf{x}_k - \nabla \mathbf{h}_k^T \mu = \mathbf{0}$$

$$\nabla_{\mu} \tilde{\mathbf{L}}^T = - \nabla \mathbf{h}_k \partial \mathbf{x}_k - \mathbf{h}_k = \mathbf{0} \tag{C.16}$$

which is identical to Equation (C.12) if

$$\mathbf{B} = \nabla_{\mathbf{x}}^2 \mathbf{L} \quad \text{and} \quad \mu = \lambda_k + \partial \lambda_k = \lambda_{k+1} \tag{C.17}$$

Thus, solving the necessary condition of Equation (C.10) via a Newton's Method is equivalent to solving the quadratic programming problem of (C.13). As a result, once we obtain the $\partial \mathbf{x}$, we can solve for the Lagrangian multiplier vector μ using Equation (C.16) and update the Lagrangian multiplier vector, λ.

Since the **B** matrix is in fact the Hessian of the Lagrangian function, it contains second order information for both the original objective function and the equality constraints. However, there are two major issues that need to be considered:

(1) The requirement to compute the Hessian matrix

(2) The ensurance of the **B** matrix to remain positive definite

To overcome these requirements, one can make use of the Davidon, Fletcher and Powell (DFP) algorithm to approximate the Hessian matrix of the Lagrangian function [44].

For the general nonlinear programming (NLP) problem with

$$\min \quad \mathbf{f}(\mathbf{x})$$

subject to

$$\mathbf{h}(\mathbf{x}) = \mathbf{0}$$
$$\mathbf{g}(\mathbf{x}) \leq \mathbf{0} \qquad \text{(C.18)}$$

one may employ the active set strategy or the slack variables to handle the inequality constraints. For more information about SQP, one should consult [45-47] for details.

APPENDIX D

TEST SYSTEMS

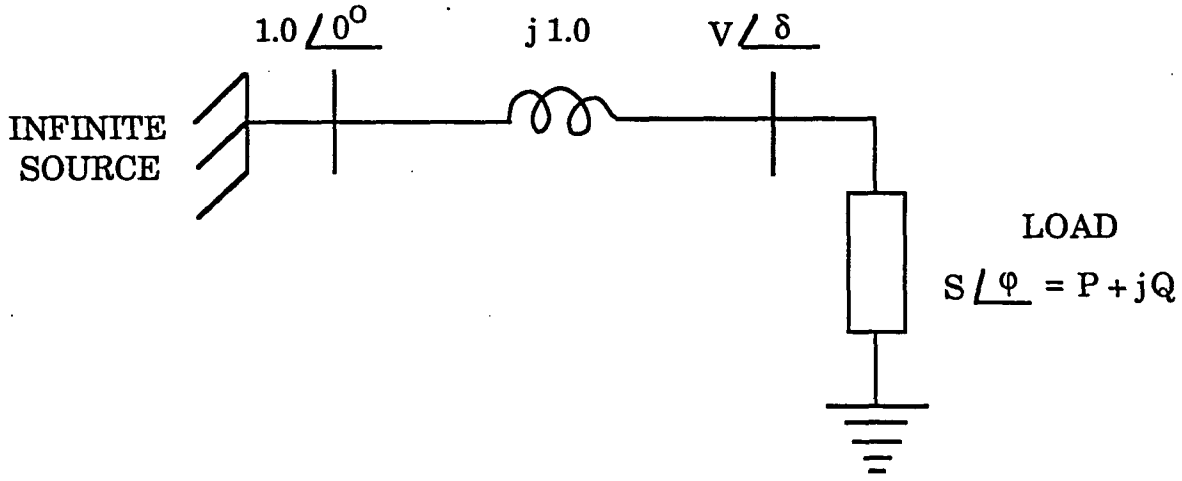

Figure D.1: 2-bus test system

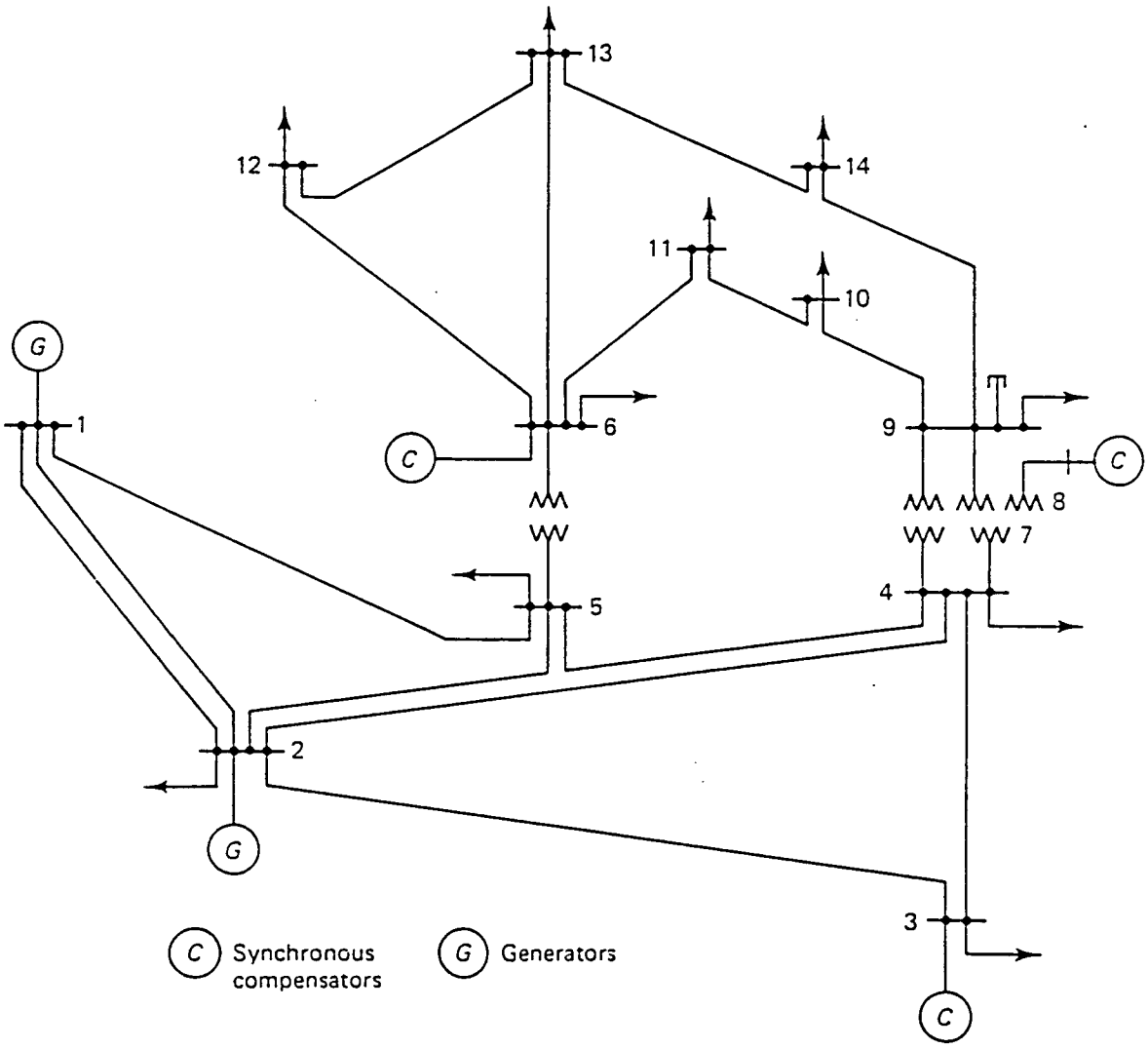

Figure D.2: AEP 14-bus test system [48]

Line designation	Resistance p.u.†	Reactance p.u.†	Line charging p.u.†
1-2	0.01938	0.05917	0.0264
1-5	0.05403	0.22304	0.0246
2-3	0.04699	0.19797	0.0219
2-4	0.05811	0.17632	0.0187
2-5	0.05695	0.17388	0.0170
3-4	0.06701	0.17103	0.0173
4-5	0.01335	0.04211	0.0064
4-7	0	0.20912	0
4-9	0	0.55618	0
5-6	0	0.25202	0
6-11	0.09498	0.19890	0
6-12	0.12291	0.25581	0
6-13	0.06615	0.13027	0
7-8	0	0.17615	0
7-9	0	0.11001	0
9-10	0.03181	0.08450	0
9-14	0.12711	0.27038	0
10-11	0.08205	0.19207	0
12-13	0.22092	0.19988	0
13-14	0.17093	0.34802	0

†Impedance and line-charging susceptance p.u. on a 100000kVA base. Line charging one-half of total charging of line.

Figure D.3: AEP 14-bus impedance and line-charging data

Bus number	Starting bus voltage		Generation		Load	
	Magnitude p.u.	Phase angle deg	MW	MVAr	MW	MVAr
1*	1.06	0	0	0	0	0
2	1.0	0	40	0	21.7	12.7
3	1.0	0	0	0	94.2	19.0
4	1.0	0	0	0	47.8	3.9
5	1.0	0	0	0	7.6	1.8
6	1.0	0	0	0	11.2	7.5
7	1.0	0	0	0	0	0
8	1.0	0	0	0	0	0
9	1.0	0	0	0	29.5	16.6
10	1.0	0	0	0	9.0	5.8
11	1.0	0	0	0	3.5	1.8
12	1.0	0	0	0	6.1	1.6
13	1.0	0	0	0	13.5	5.8
14	1.0	0	0	0	14.9	5.6

*Swing machine

Figure D.4: AEP 14-bus test system - operating conditions

Bus number	Voltage magnitude, p.u.	Minimum MVAr capability	Maximum MVAr capability
2	1.045	−40	50
3	1.010	0	40
6	1.070	−6	24
8	1.090	−6	24

Figure D.5: AEP 14-bus test system - regulated bus data

Transformer designation	Tap setting
4-7	0.978
4-9	0.969
5-6	0.932

Figure D.6: AEP14-bus test system - transformer data

Bus number	Susceptance† p.u.
9	0.19

†Susceptance p.u. on a 100000kVA base.

Figure D.7: AEP 14-bus test system - static capacitor data

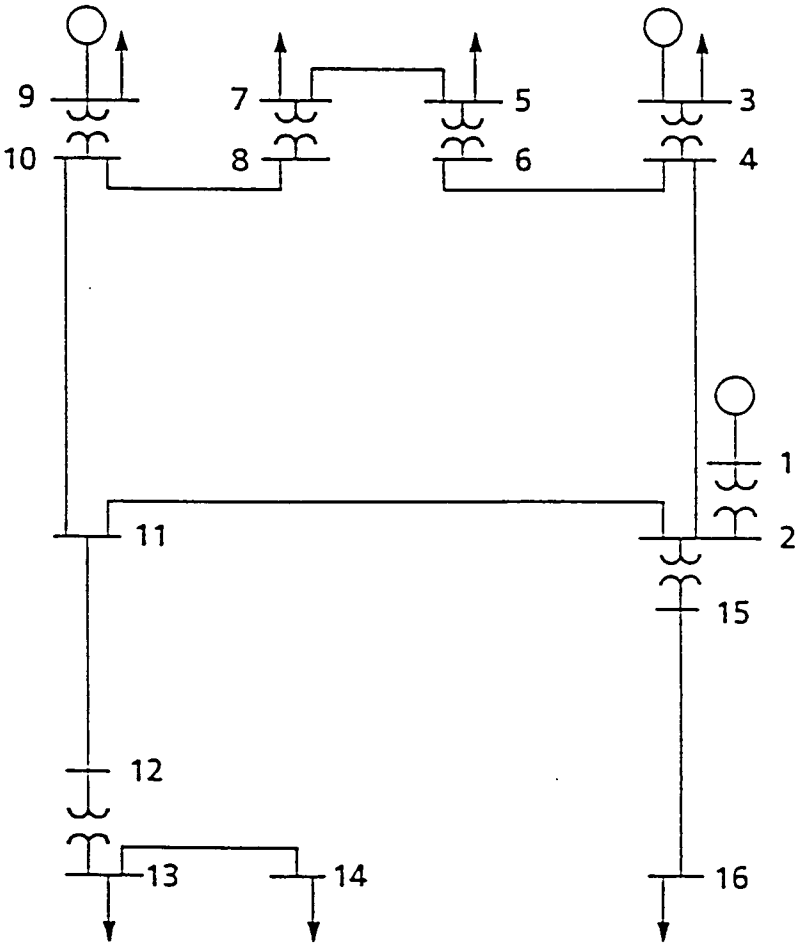

Figure D.8: 16-bus test system [39]

Line Data

Bus-Bus		R	X	B	S_{Rating}
4	6	0.006650	0.035190	0.074580	3.585
8	10	0.006650	0.035190	0.074580	3.585
10	11	0.009980	0.052790	0.111900	3.585
2	4	0.016640	0.087980	0.186440	3.585
2	11	0.016640	0.087980	0.186440	3.585
5	7	0.008302	0.045550	0.008129	2.012
15	16	0.027680	0.151800	0.027100	2.012
11	12	0.006656	0.035192	0.074576	3.585
13	14	0.052100	0.177300	0.003707	0.372

Transformer Data

Bus-Bus		Type	R	X	S_{Rating}	Tap
1	2	Fix	0.003500	0.035000	2.000	1.0000
15	2	Fix	0.002722	0.032670	2.000	1.0000
13	12	Fix	0.002083	0.041670	1.200	1.0250
3	4	Fix	0.003846	0.038460	1.300	1.0000
5	6	Fix	0.001667	0.041670	1.200	1.0000
7	8	Fix	0.001667	0.041670	1.200	1.0000
9	10	Fix	0.001200	0.024000	2.500	1.0000

System Load

Bus	$P_{3\phi}$ (MW)	$Q_{3\phi}$ (Mvar)
1	—	—
2	0	0
3	10	55
4	0	0
5	75	15
6	0	0
7	90	20
8	0	0
9	15	4
10	0	0
11	0	0
12	0	0
13	50	2
14	35	3
15	0	0
16	150	20

Figure D.9: 16-bus test system - line, transformer and system load data

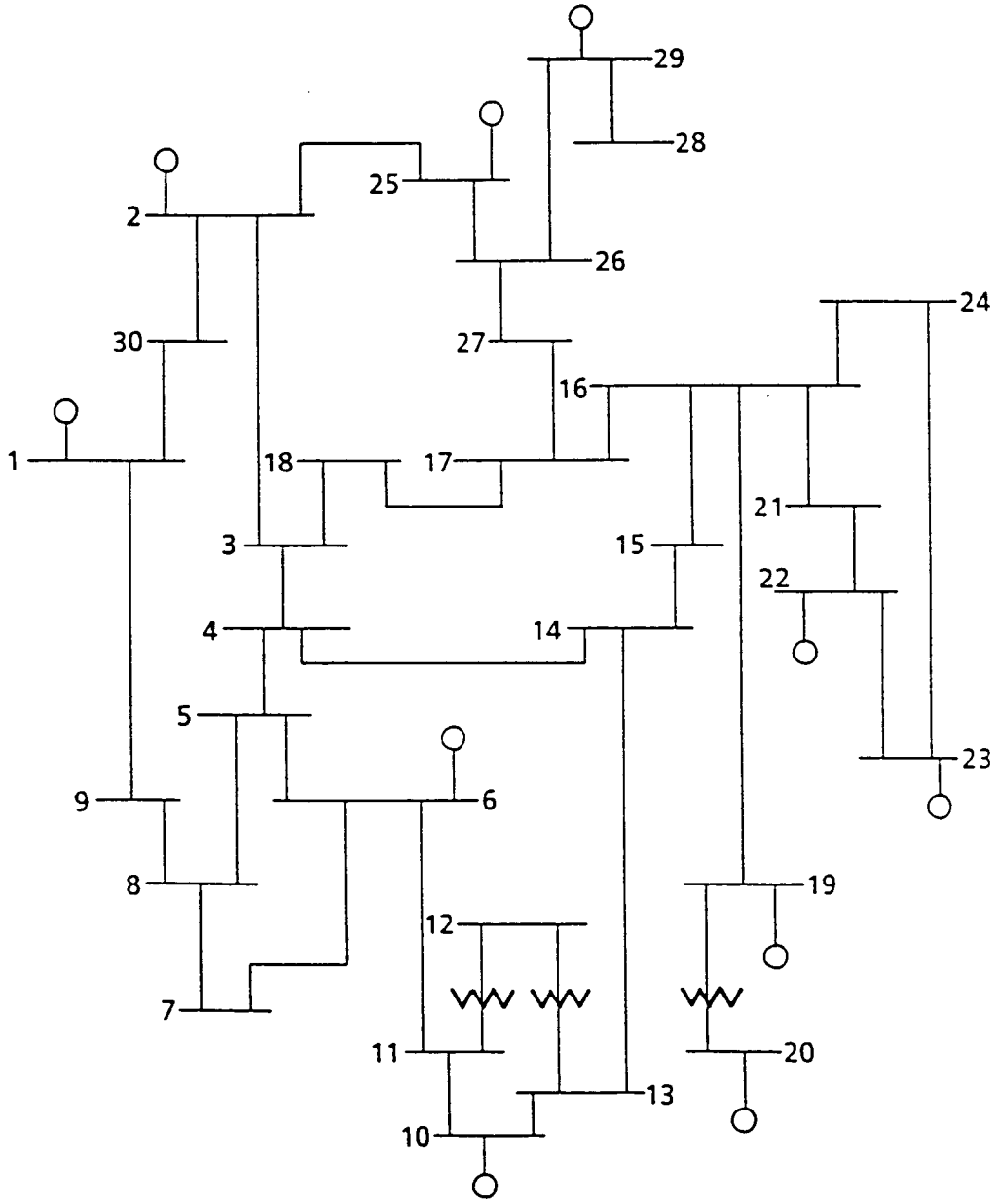

Figure D.10: New England 30-bus test system [49]

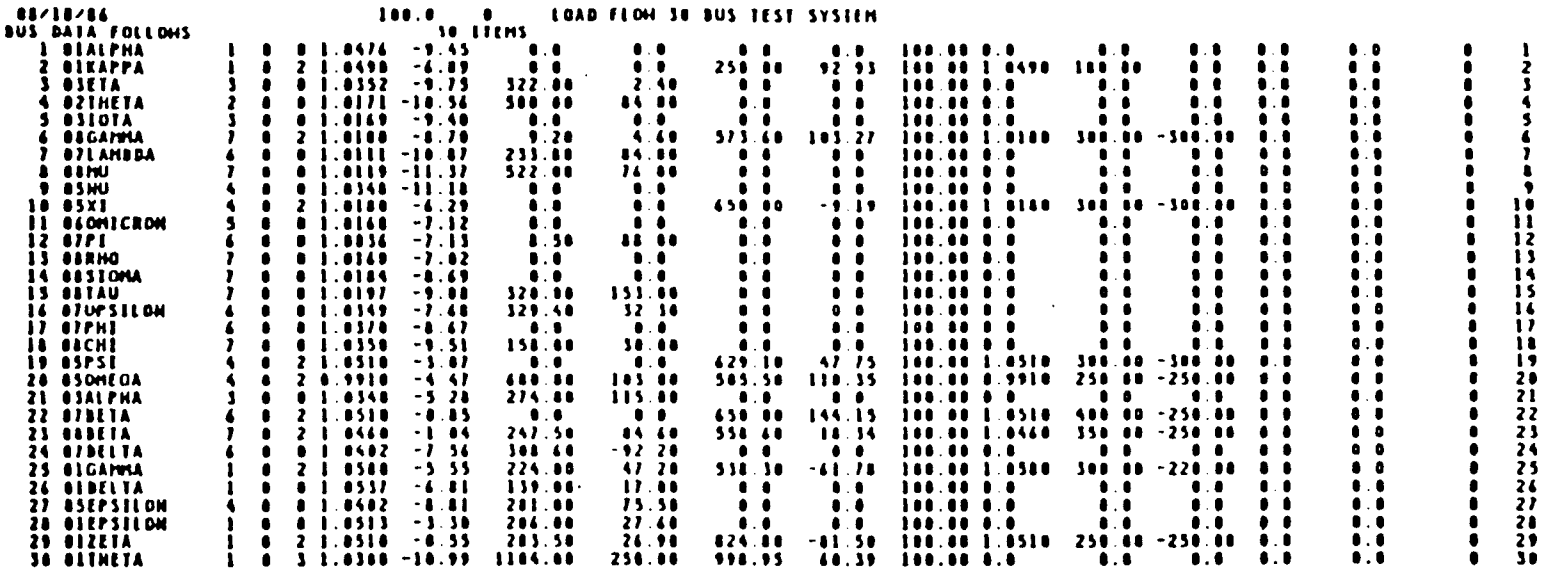

```
 08/18/86                    100.0    0     LOAD FLOW 30 BUS TEST SYSTEM
BUS DATA FOLLOWS                  30 ITEMS
   1 01ALPHA     1   0   0  1.0474   -9.45      0.0        0.0        0.0        0.0     100.00  0.0        0.0        0.0        0.0        0.0        0   1
   2 01KAPPA     1   0   2  1.0498   -6.09      0.0        0.0      256.88      92.93     100.00  1.0498   100.00       0.0        0.0        0.0        0   2
   3 03ETA       3   0   0  1.0352   -9.75    322.00       2.40       0.0        0.0       100.00  0.0        0.0        0.0        0.0        0.0        0   3
   4 02THETA     2   0   0  1.0171  -10.56    500.00      84.00       0.0        0.0       100.00  0.0        0.0        0.0        0.0        0.0        0   4
   5 03IOTA      3   0   0  1.0169   -9.40      0.0        0.0        0.0        0.0       100.00  0.0        0.0        0.0        0.0        0.0        0   5
   6 06GAMMA     7   0   2  1.0100   -8.78      9.20       4.60     573.60     103.27     100.00  1.0100   300.00    -300.00       0.0        0.0        0   6
   7 07LAMBDA    6   0   0  1.0111  -10.07    233.80      84.00       0.0        0.0       100.00  0.0        0.0        0.0        0.0        0.0        0   7
   8 08MU        7   0   0  1.0119  -11.37    522.00      74.00       0.0        0.0       100.00  0.0        0.0        0.0        0.0        0.0        0   8
   9 05NU        4   0   0  1.0348  -11.18      0.0        0.0        0.0        0.0       100.00  0.0        0.0        0.0        0.0        0.0        0   9
  10 05XI        4   0   2  1.0100   -6.29      0.0        0.0      650.00      -9.19     100.00  1.0100   300.00    -300.00       0.0        0.0        0  10
  11 06OMICRON   5   0   0  1.0148   -7.12      0.0        0.0        0.0        0.0       100.00  0.0        0.0        0.0        0.0        0.0        0  11
  12 07PI        6   0   0  1.0036   -7.13      8.50      88.00       0.0        0.0       100.00  0.0        0.0        0.0        0.0        0.0        0  12
  13 08RHO       7   0   0  1.0149   -7.02      0.0        0.0        0.0        0.0       100.00  0.0        0.0        0.0        0.0        0.0        0  13
  14 08SIGMA     7   0   0  1.0184   -8.69      0.0        0.0        0.0        0.0       100.00  0.0        0.0        0.0        0.0        0.0        0  14
  15 08TAU       7   0   0  1.0197   -9.08    320.00     153.00       0.0        0.0       100.00  0.0        0.0        0.0        0.0        0.0        0  15
  16 07UPSILON   6   0   0  1.0349   -7.48    329.40      32.10       0.0        0.0       100.00  0.0        0.0        0.0        0.0        0.0        0  16
  17 07PHI       6   0   0  1.0370   -8.67      0.0        0.0        0.0        0.0       100.00  0.0        0.0        0.0        0.0        0.0        0  17
  18 08CHI       7   0   0  1.0358   -9.51    158.00      30.00       0.0        0.0       100.00  0.0        0.0        0.0        0.0        0.0        0  18
  19 05PSI       4   0   2  1.0510   -3.87      0.0        0.0      629.10      47.75     100.00  1.0510   300.00    -300.00       0.0        0.0        0  19
  20 05OMEGA     4   0   2  0.9910   -4.47    680.00     103.00     505.50     118.35     100.00  0.9910   250.00    -250.00       0.0        0.0        0  20
  21 03ALPHA     3   0   0  1.0348   -5.28    274.00     115.00       0.0        0.0       100.00  0.0        0.0        0.0        0.0        0.0        0  21
  22 07BETA      6   0   2  1.0510   -8.85      0.0        0.0      650.00     144.15     100.00  1.0510   400.00    -250.00       0.0        0.0        0  22
  23 08DETA      7   0   2  1.0460   -1.04    247.50      84.60     550.60      18.34     100.00  1.0460   350.00    -250.00       0.0        0.0        0  23
  24 07DELTA     6   0   0  1.0402   -7.56    308.60     -92.20       0.0        0.0       100.00  0.0        0.0        0.0        0.0        0.0        0  24
  25 01GAMMA     1   0   2  1.0580   -5.55    224.00      47.20     538.30     -61.78     100.00  1.0580   300.00    -220.00       0.0        0.0        0  25
  26 01DELTA     1   0   0  1.0537   -6.81    139.00      17.00       0.0        0.0       100.00  0.0        0.0        0.0        0.0        0.0        0  26
  27 05EPSILON   4   0   0  1.0402   -8.81    281.00      75.50       0.0        0.0       100.00  0.0        0.0        0.0        0.0        0.0        0  27
  28 01EPSILON   1   0   0  1.0513   -3.30    206.00      27.60       0.0        0.0       100.00  0.0        0.0        0.0        0.0        0.0        0  28
  29 01ZETA      1   0   2  1.0510   -0.55    283.50      26.90     824.80     -81.50     100.00  1.0510   250.00    -250.00       0.0        0.0        0  29
  30 01THETA     1   0   3  1.0300  -10.99   1106.00     250.00     998.95      60.39     100.00  0.0        0.0        0.0        0.0        0.0        0  30
```

Figure D.11: New England 30-bus test system - bus data

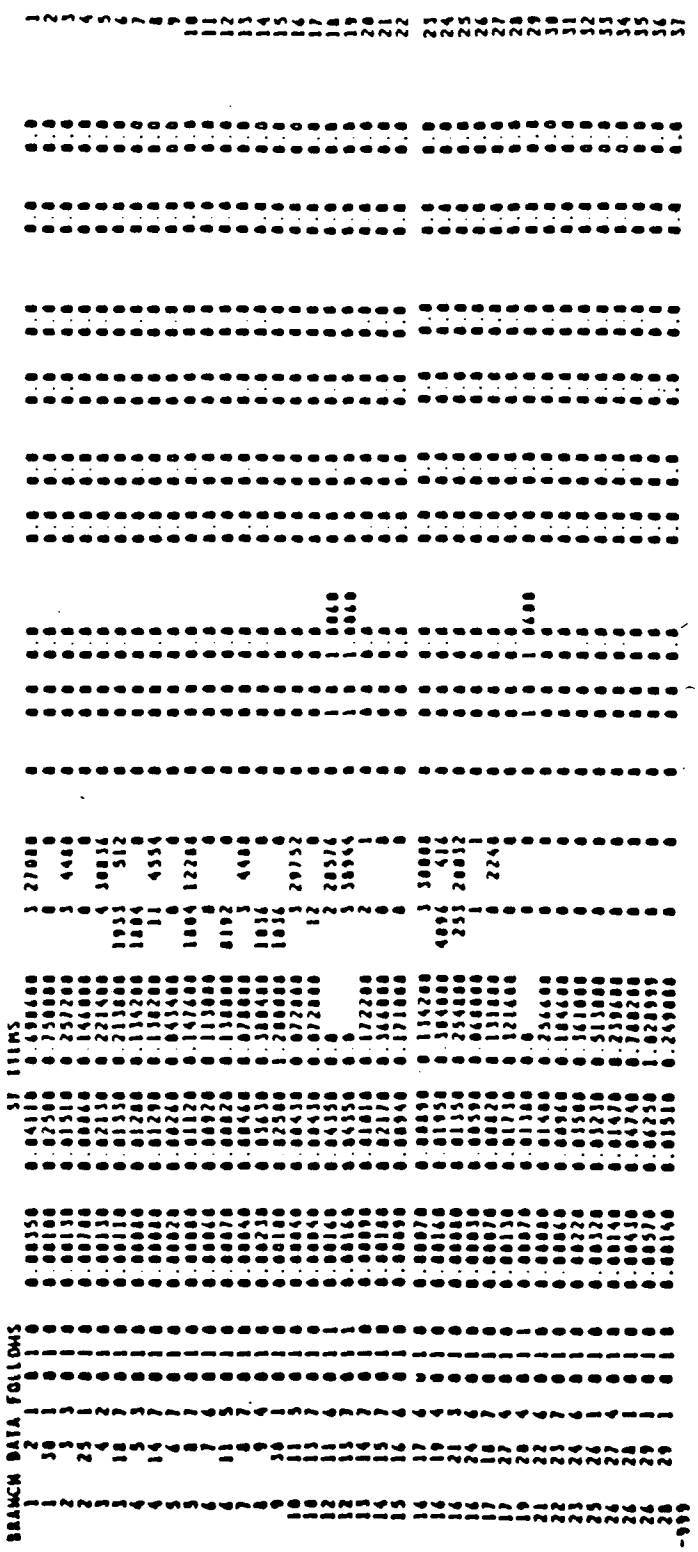

Figure D.12: New England 30-bus test system - branch data